Lecture Notes on

Langmuir Probe Diagnostics

Francis F. Chen

Electrical Engineering Department
University of California, Los Angeles

Mini-Course on Plasma Diagnostics, IEEE-ICOPS meeting, Jeju, Korea, June 5, 2003

TABLE OF CONTENTS

INTRODUCTION

Of all the ways to measure a plasma, the Langmuir probe is probably the simplest, since it consists of sticking a wire into the plasma and measuring the current to it at various applied voltages. However, it is an intrusive, not remote, technique; and the "wire" must be carefully designed so as not to interfere with the plasma nor be destroyed by it. Worse than that, the interpretation of the current-voltage ($I - V$) curves is difficult and has spawned a large literature of theoretical papers. In a short lecture, little of this can be discussed in detail. Specialized topics and related electrostatic diagnostics, such as emissive probes, double probes, capacitive probes, oscillation probes, probes in flowing or high pressure plasmas, and probes in a magnetic field can be mentioned only summarily.

On the other hand, the most widespread use of Langmuir probes at present is in the semiconductor industry, where radiofrequency (rf) sources are used to produce plasmas for etching and deposition. These partially ionized plasmas require special techniques in probe construction and theory. Emphasis will be given to this new forefront of diagnostics research.

GENERAL REFERENCES

F.F. Chen, *Electric Probes*, in "Plasma Diagnostic Techniques", ed. by R.H. Huddlestone and S.L. Leonard (Academic Press, New York), Chap. 4, pp. 113-200 (1965).

L. Schott, *Electrical Probes*, in "Plasma Diagnostics", ed. by W. Lochte-Holtgreven (John Wiley, New York, 1968), Chap. 11.

J.D. Swift and M.J.R. Schwar, "Electrical Probes for Plasma Diagnostics" (Elsevier, New York, 1969).

P.M. Chung, L. Talbot, and K.J. Touryan, "Electric Probes in Stationary and Flowing plasmas" (Springer-Verlag, New York, 1975).

I.M. Hutchinson, "Principles of Plasma Diagnostics" (Cambridge Univ. Press, Cambridge, 1987), Chap. 3.

N. Hershkowitz, *How Langmuir Probes Work*, in "Plasma Diagnostics", Vol. 1, ed. by O. Auciello and D.L. Flamm (Academic Press, Boston, 1989), Chap. 3.

I. THE PROBE CHARACTERISTIC

A. Parts of the *I – V* curve

Let the plasma potential (space potential) be V_s, and the potential applied to the probe be V_p. If the chamber walls are metal and grounded, V_s is normally of the order of $5KT_e$. When $V_p >> V_s$, an electron current I_e is collected; the probe current is negative. When $V_p << V_s$, an ion current I_i is collected. It is customary to plot $I - V$ curves with I_e positive and I_i negative. Such a plot is shown in Fig. 1. There are five main parts.

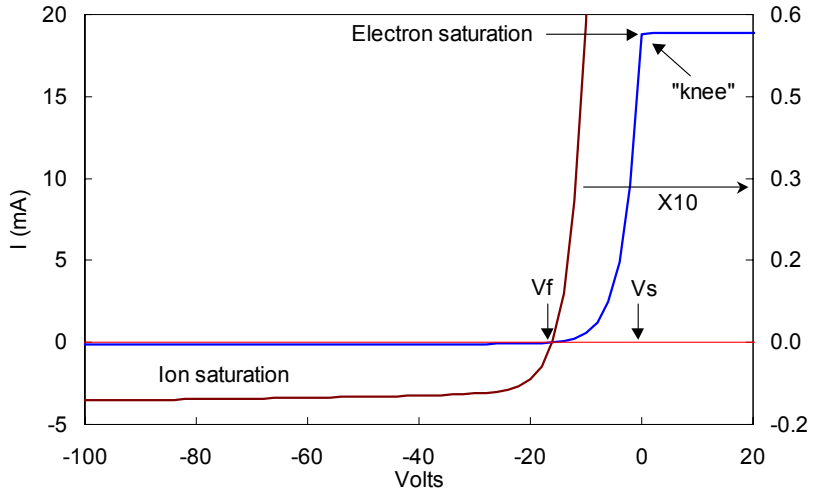

Fig. 1. An idealized $I - V$ curve. The left curve is expanded 10X to show the ion current.

The space potential V_s is near the "knee" of the curve. At the far left, where all the electrons have been repelled, we have the Ion Saturation current, I_{sat}. The Floating Potential V_f, is where the ion and electron currents are equal, and the net current is zero. In the Transition Region, the ion current is negligible, and the electrons are partially repelled by the negative potential $V_p – V_s$. In a Maxwellian plasma, this part of the curve is exponential. When V_p (or just V) reaches V_s, all of the random thermal flux of electrons is collected. In the Electron Saturation region, I_e grows only slowly because of the expansion of the sheath. From the $I – V$ curve, the plasma density n, electron temperature KT_e, and plasma potential V_s can be determined, *but not the ion temperature*.

B. The Transition Region

The exponential part of the *I-V* curve, when plotted semi-logarithmically vs. the probe voltage V_p, should be a straight line if the electrons are Maxwellian:

$$I_e = I_{es} \exp[e(V_p - V_s)/KT_e)], \tag{1}$$

where

$$I_{es} = eAn_e\bar{v}/4 = en_eA\left(\frac{KT_e}{2\pi m}\right)^{1/2}, \tag{2}$$

A being the exposed area of the probe tip. Here I_{es} is the saturation electron current, or random thermal current to a surface at V_s. Eq. (1) shows that the slope of the (ln I)–V_p curve is exactly $1/T_{eV}$ and is a good measure of the electron temperature. (It is convenient to write

KT_e/e as T_{eV}, the electron temperature in eV). This is a very robust relationship, and T_e is the easiest quantity to obtain from a probe. As long as the electrons are Maxwellian and are repelled by the probe, the EEDF at a potential $V < 0$ is proportional to

$$f(\mathrm{v}) \propto \mathrm{e}^{-(\frac{1}{2}m\mathrm{v}^2+eV)/KT_e} = \mathrm{e}^{-e|V|/KT_e}\mathrm{e}^{-(m\mathrm{v}^2/2KT_e)}. \qquad (3)$$

We see that f(v) is still Maxwellian at the same T_e; only the density is decreased by $\exp(-e|V|/KT_e)$. Thus, the slope of the semilog curve is independent of probe area or shape and independent of collisions, since these merely preserve the Maxwellian distribution. However, before I_e can be obtained from I, one has to subtract the ion current I_i. This can be done approximately by drawing a straight line through I_{sat} and extrapolating it to the electron region.

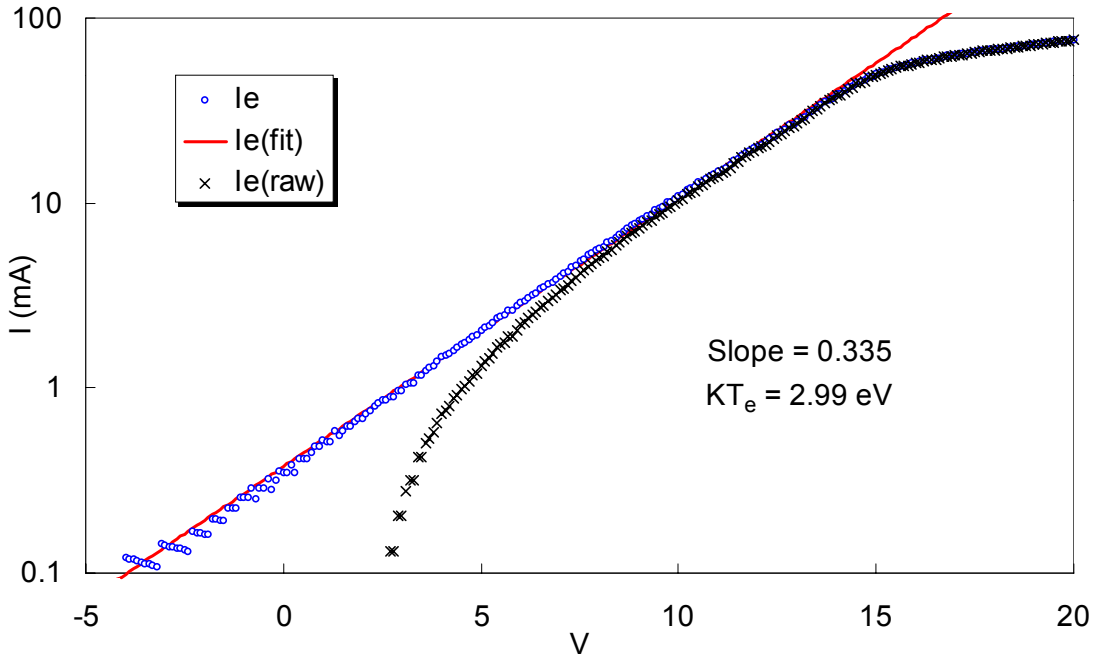

Fig. 1. A semilog plot of electron current from an $I - V$ curve in an rf plasma. The lower curve is the raw data before the ion current is subtracted from the total current.[1]

One can estimate the ion contribution more accurately by using one of the theories of ion collection discussed below, but refinements to this small correction are usually not necessary, and they affect only the high-energy tail of the electron distribution. One easy iteration is to change the magnitude of the I_{sat} correction until the ln I plot is linear over as large a voltage range as possible. Fig. 1 shows a measured electron characteristic and a straight-line fit to it. The ion current was calculated from a theoretical fit to I_{sat} and added back to I to get I_e. The uncorrected points are also shown; they have a smaller region of linearity. If the EEDF (Electron Energy Distribution Function) is not Maxwellian, $f(v)$ can sometimes be determined from the shape of this curve. This will be discussed later.

C. Electron saturation

The exponential growth of I_e with V_p should continue until $V_p = V_s$, when none of the electrons is repelled by a negative potential. The electron current "saturates". Since the electron velocities are $\approx(m/M)^{1/2}$ times larger than ion velocities, one would expect I_{es} to be >200 times as large as I_{sat} (in argon). In low-pressure, unmagnetized, dc discharges, this is indeed

true[2]; the knee of the curve is sharp and is a good measure of V_s. For $V_p > V_s$, I_e increases slowly as the collection area grows due to an increase in sheath thickness, the shape of the curve depending on the shape of the probe tip. One might think that measurement of I_{es} would give information on the electron density, but this is possible only at low densities and pressures, where the mean free path is very long. Otherwise, the current collected by the probe is so large that it drains the plasma and changes its equilibrium properties. It is better to measure n by collecting ions, which would give the same information, since plasmas are quasineutral. More importantly, one should avoid collecting saturation electron current for more than a few milliseconds at a time, because the probe can be damaged.

However, this ideal situation is rarely found in practical devices. Effects such as collisions and magnetic fields will lower the magnitude of I_{es} and round off the knee so that V_s is hard to determine. In particular, magnetic fields strong enough to make the electron Larmor radius smaller than the probe radius will limit I_{es} to only 10-20 times I_{sat} because the probe depletes the field lines that it intercepts, and further electrons can be collected only if they diffuse across the B-field. The knee, now indistinct, indicates a space potential, but only that in the depleted tube of force, not V_s in the main plasma. In this case, the $I - V$ curve is exponential only over a range of a few KT_e above the floating potential and therefore samples only the electrons in the tail of the Maxwellian. Figure 2 shows an $I - V$ curve in a magnetized plasma, where the knee is just a small bend occurring where I_e is only 10-30 times the ion current.

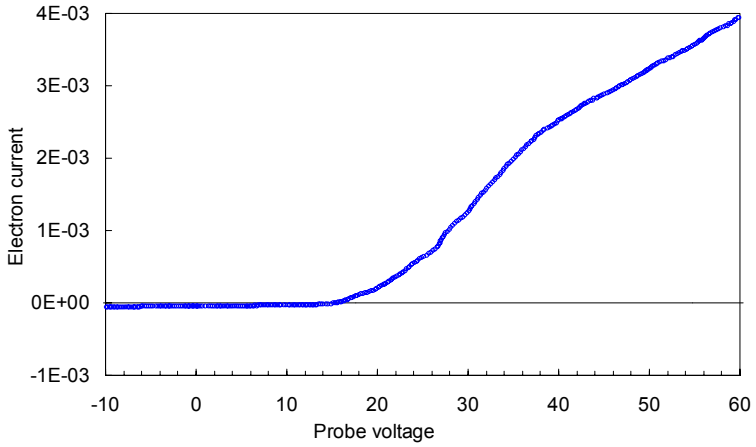

Fig. 2. Example of an $I - V$ curve in a magnetized, rf plasma.

Collisions can also limit I_{es}. In the high-pressure limit, electrons must diffuse through the neutral gas to reach the sheath edge, so the current there is limited by the diffusion rate. In rf plasmas, $V_s - V_p$ can fluctuate at the rf frequency, and electron collection depends on the phase and velocity of the electron when it enters the sheath. An example of an $I - V$ curve in an unmagnetized rf plasma is shown in Fig. 3.a Here electron saturation begins at I_e not much larger than the maximum ion current. The curve is linear only over a relatively small current range. This range is reduced even further by the presence of a fast electron population. Figure 4. shows such a case. The electron tail can distort the apparent electron temperature of the bulk. This will be discussed in a later section. In Fig. 3b, electron saturation current increases linearly from the knee to the value I_{es} should have. The reason for this is not yet known.

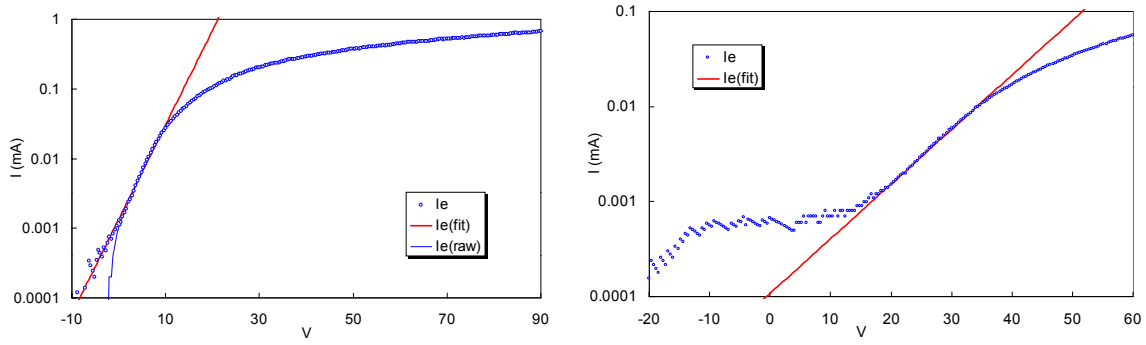

Fig.3. Example of an $I - V$ curve in an unmagnetized rf plasma (a) with and (b) without fast electrons[1].

D. Floating potential

The potential V_f is defined by $I_i = I_e$, where I_e is given by Eqs. (1) and (2) if the electrons are Maxwellian. I_i can be calculated from one of the theories presented in a later section but for this purpose can be estimated from the Bohm current[3]

$$I_B = \alpha neAc_s, \quad c_s \equiv (KT_e/M)^{1/2}, \quad \alpha \approx 0.5, \tag{4}$$

where M is the *ion* mass. This current is caused by the electric field in the presheath which accelerates ions to a velocity of c_s, the minimum required to form a sheath. Setting Eqs. (1) and (4) equal yields

$$V_f = V_s - \frac{KT_e}{2e}\ln\left(\frac{2M}{\pi m}\right). \tag{5}$$

The value of $V_f - V_s$ is about $-3.5T_{eV}$ for hydrogen and $-5.4T_{eV}$ for argon. V_f is more negative than this if there are fast "primary" electrons or if there are uncompensated rf fields. Strictly speaking, Eq. (4) applies only to plane probes. For cylindrical probes there is a

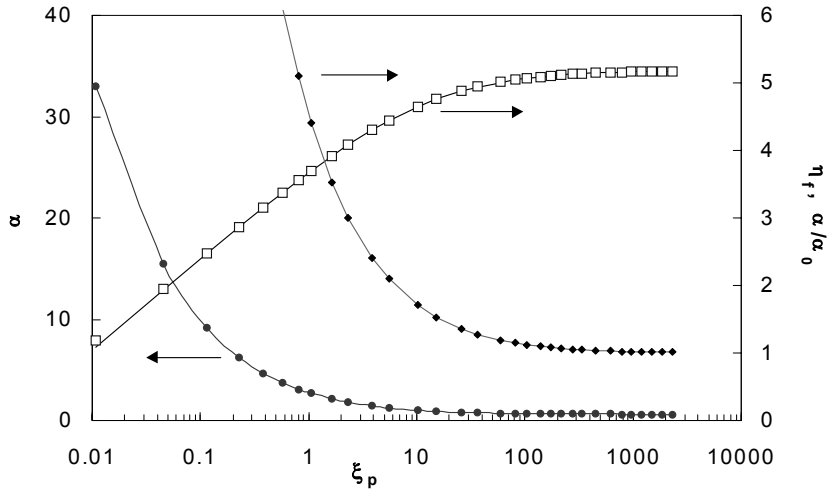

Fig. 4. Decrease of V_f for cylinders from its asymptotic value as ξ_p is decreased. The effective Bohm coefficient α is also shown, as well as its value normalized to $\alpha_0 = 0.61$.

geometrical correction[4] which lowers the value of $-5.4T_{eV}$ to between -4 and $-5T_{eV}$, depending on the ratio of probe radius to Debye length. The function $V_f(\xi_p)$ is shown in Fig. 4, where $\eta_f = eV_f/KT_e$. An analytic fit to this curve is given by

$$\frac{1}{(\eta_f)^6} = \frac{1}{(A\ln\xi_p + B)^6} + \frac{1}{(C\ln\xi_p + D)^6} \tag{6}$$

where $A = 0.583$, $B = 3.732$, $C = -0.027$, and $D = 5.431$.

E. Space potential

The time-honored way to obtain the space potential (or plasma potential) is to draw straight lines through the $I - V$ curve in the transition and electron saturation regions and call the crossing point V_s, I_{es}. This does not work well if I_{es} is curved, as in Fig. 3a. In that case, there are two methods one can use. The first is to measure V_f and calculate V_s from Eq. (5). The second is to take the point where I_e starts to deviate from exponential growth; that is, where $I_e'(V)$ is maximum or $I_e''(V)$ is zero. If $I_e'(V)$ has a distinct maximum, a reasonable value for V_s is obtained, as illustrated in Fig. 5.

It would be dangerous to equate the current there to I_{es} in order to compute n_e, for two reasons. First, the knee can occur before V_s is reached, as in Fig. 3. Second, according to Eq.(1), I_{es} depends exponentially on the assumed value of V_s, so that a small error in V_s would induce a large error in the inferred value of n. The only sure way to measure V_s is to use a hot, or emitting, probe[5], for which $V_f \approx V_s$.

In magnetized plasmas, which frequently have low-frequency oscillations, fluctuations in V_f. can be measured with a floating probe. If KT_e does not vary, the V_s spectrum should be the same as the V_f spectrum. Methods have been devised to separate

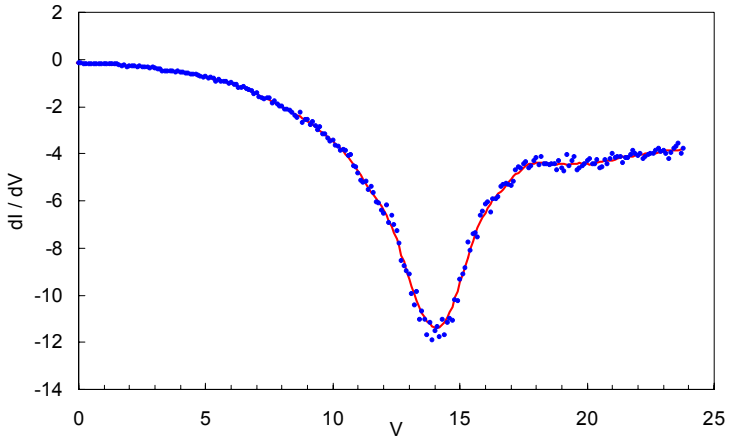

Fig. 5. Derivative of an $I - V$ curve that has a distinct minimum at V_s.

$\tilde{V}_s$ from $\tilde{T}_e$ by using baffled probes which block most of the electron current to a floating probe[6]. Using a floating hot probe would be better, but it would be difficult to neutralize the large capacitance of the heating circuit. Floating probes must be terminated in a high impedance, and the RC time constant of this resistor and the stray capacitance can limit the frequency response.

F. Ion saturation current

We have seen that measuring n with electron saturation current can be quite inaccurate and could draw dangerously large probe currents in a dense plasma. Saturation ion currents are much smaller and easier to handle because of the low output impedance that they provide. Unfortunately, interpretation of the I_{sat} curve requires major computation, and the

results can also be quite inaccurate. Only on a good day can one measure n to within 10% using I_{sat}. Here we present the simplest approximation, appropriate for plane probes or probes with large ξ_p, where ξ_p is the ratio between probe radius and Debye length:

$$\xi_p \equiv R_p / \lambda_D , \qquad \lambda_D^2 \equiv \varepsilon_0 K T_e / ne^2 . \tag{7}$$

Cylindrical probe theory will be discussed in a separate section. Spherical probes are the easiest to treat theoretically, but they are impractical to make.

At densities above about 10^{11} cm^{-3}, the sheath around a negatively biased probe is so thin that the area of the sheath edge is essentially the same as the area of the probe tip itself. The ion current is then just that necessary to satisfy the Bohm sheath criterion of Eq. (4), where the factor α represents n_s/n, the density at the sheath edge relative to the density in the main plasma. The coefficient α, is only approximately 0.5; when probes are calibrated against other diagnostics, such as microwave interferometry, α = 0.6-0.7 has been found to be more accurate. The theoretical value is $\alpha = \exp(-1/2) = 0.61$. Note that Eq. (4)predicts a constant I_{sat}, which can happen only for flat probes in which the sheath area cannot expand as the probe is made more and more negative. In practice, I_{sat} usually has a slope to it. This is because the ion current has to come from a disturbed volume of plasma (the presheath) where the ion distribution changes from isotropic to unidirectional. If the probe is a disk of radius R, say, the disturbed volume may have a size comparable to R, and would increase as the $|V_p|$ increases. In that case, one can extrapolate I_i back to V_f to get a better measure of I_{sat} before the expansion of the presheath. This is illustrated in Fig. 6. Saturation is quite good

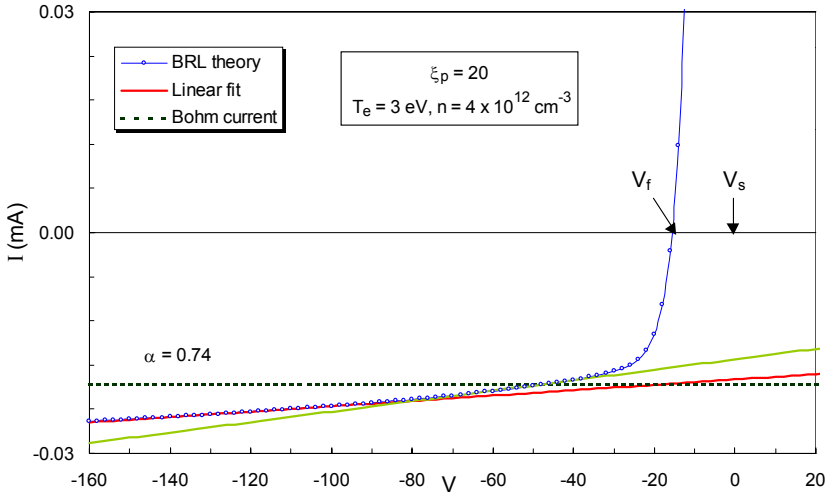

Fig. 6. Extrapolation of I_{sat} to $V = V_f$ for a probe with $\xi_p - 20$. If the current there is equated to the Bohm current, the Bohm coefficient would have to be 0.74.

in this example, since I_{sat} changes little over 80V in V_p. The curve, however, is based on collisionless theory, and may not agree with experiment. As ξ_p is varied, the value of α that one must use in applying the Bohm formula to a cylindrical probe would change as shown in Fig. 7. Better saturation with a plane probe can be obtained by using a *guard ring*, a flat washer-shaped disk surrounding the probe but not touching it. It is biased at the same potential as the probe to keep the fields planar as V_p is varied. The current to the guard ring is disregarded. A section of the chamber wall can be isolated to be used as a plane probe with a large guard ring.

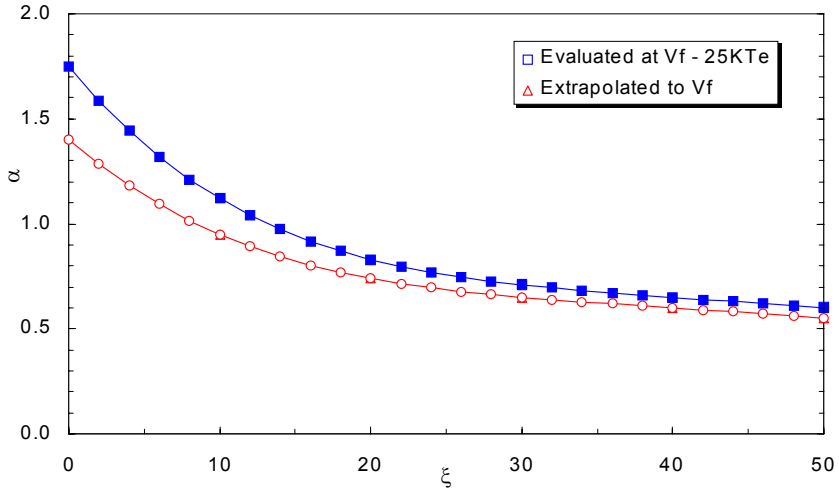

Fig. 7. The required values of α to use in the Bohm formula in order to fit I_{sat} at V_f to the theoretical value for a cylindrical probe.

II. DESIGN OF PROBES AND CIRCUITS FOR RF ENVIRONMENTS

A. Probe construction

Since the probe is immersed in a harsh environment, special techniques are used to protect it from the plasma and vice versa, and to ensure that the circuitry gives the correct I – V values. The probe tip is made of a high-temperature material, usually a tungsten rod or wire 0.1–1 mm in diameter. The rod is threaded into a thin ceramic tube, usually alumina, to insulate it from the plasma except for a short length of exposed tip, about 2–10 mm long. These materials can be exposed to low-temperature laboratory plasmas without melting or excessive sputtering. To avoid disturbing the plasma, the ceramic tube should be as thin as possible, preferably < 1 mm in diameter but usually several times this. The probe tip should be centered in the tube and extend out of its end without touching it, so that it would not be in electrical contact with any conducting coating that may deposit onto the insulator. The assembly is encased in a vacuum jacket, which could be a stainless steel or glass tube 1/4″ in outside diameter (od). It is preferable to make the vacuum seal at the outside end of the probe assembly rather than at the end immersed in the plasma, which can cause a leak. Ideally, only the ceramic part of the housing should be allowed to enter the plasma. Some commercial Langmuir probes use a rather thick metal tube to support the probe tip assembly, and this can modify the plasma characteristics unless the density is very low. In dense plasmas the probe cannot withstand the heat unless the plasma is pulsed or the probe is mechanically moved in and out of the plasma in less than a second. When collecting ion current, the probe can be eroded by sputtering, thus changing its collection area. This can be minimized by using carbon as the tip material. Ordinary pencil lead, 0.3mm in diameter works well and can be supported by a hypodermic needle inside the ceramic shield. One implementation of a probe tip assembly is shown in Fig. 8. An example of a right-angled

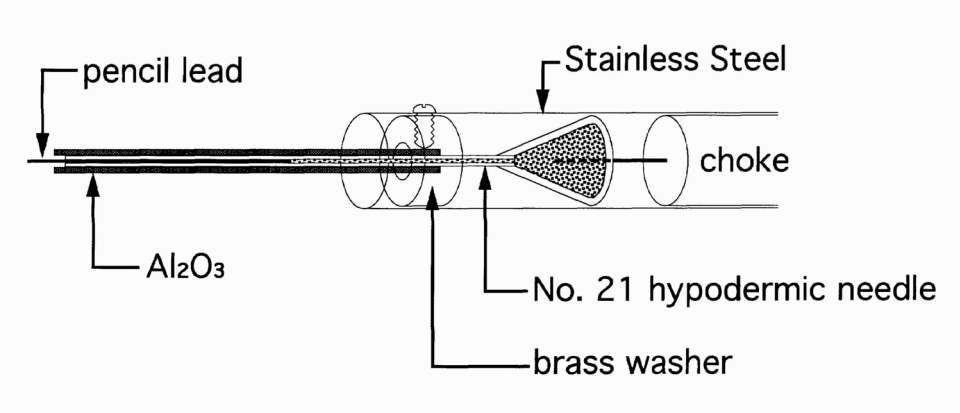

Fig. 8. A carbon probe tip assembly with rf compensation circuitry [Ref. 7].

probe with rf compensation circuitry is shown in Fig. 9. Commercial probes are available from Hiden Analytical and Scientific Systems, among others. The probe tip assembly of the

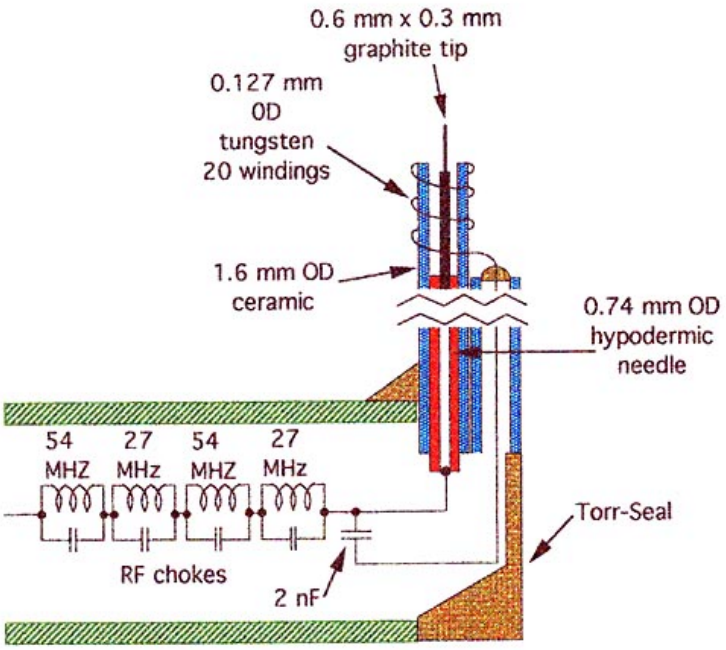

Fig. 9. A right-angled probe with rf compensation for 27MHz [Ref. 7].

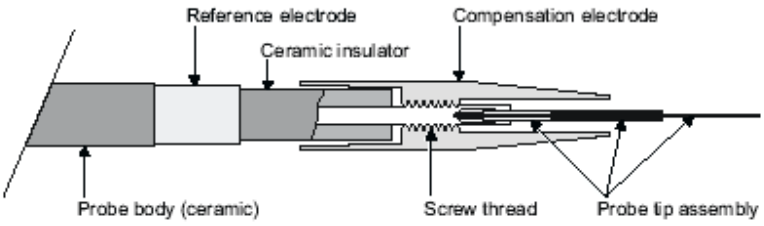

Fig. 10. Probe tip assembly in the Hiden Analytical ESPion system.

Hiden system is shown in Fig. 10. This has replaceable probe tips, well centered, and an extremely large auxiliary electrode (described later).

A flat probe would seem to the simpler, since it would just draw the Bohm current and the sheath area would not change with probe bias. However, the current has to come from somewhere. In order for the probe not to disturb the plasma, the surface from which the current comes must be much larger than the probe surface. In that case, the probe acts like a spherical probe, and the current will not saturate. The disturbance is minimized if the flat probe is part of a wall, but changing the probe bias would still affect the collection area. The planarity of the collecting surface can be improved by adding a guard ring, co-planar with the probe and biased to the same V_p. The current to the guard ring is affected by edge effects, but it is not measured. Only the current to the central probe area with a planar sheath is measured. An example of a plane probe is shown in Fig. 10. Figure 11 shows such a probe and guard-ring system mounted as part of a wall.

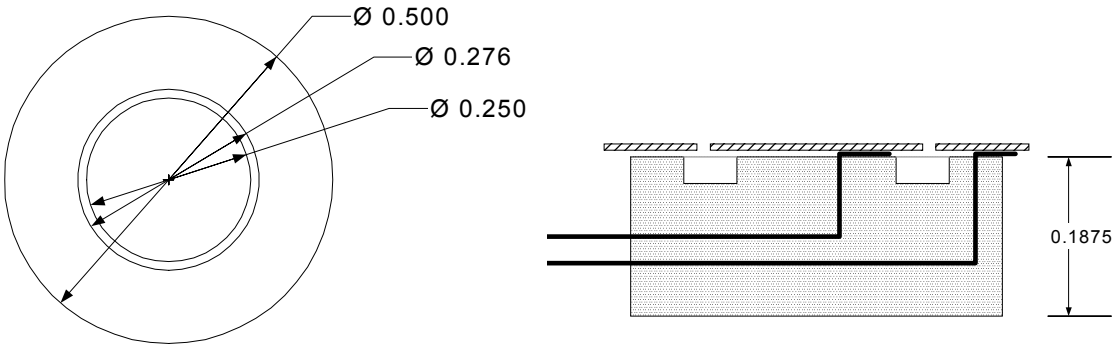

Fig. 10 A flat probe with guard ring.

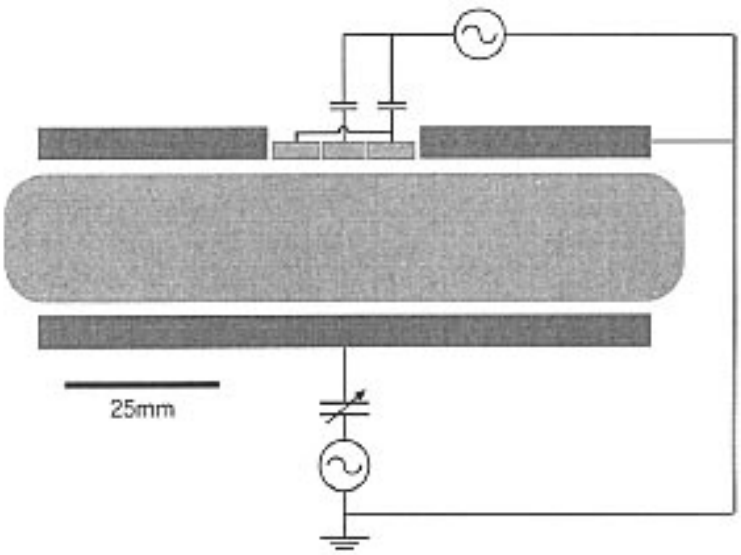

Fig. 11. A flat probe with guard ring mounted on the grounded electrode of a capacitive discharge [Ref. 8].

B. Probe circuits

There are two basic ways to apply a voltage V to the probe and measure the current I that it draws from the plasma, and each has its disadvantages. In Fig. 12a, the probe lead, taken through a vacuum fitting, is connected to a battery or a variable voltage source (*bias supply*) and then to a termination resistor R to ground. To measure the probe current, the

voltage across R is recorded or displayed on an oscilloscope. This arrangement has the advantage that the measuring resistor is grounded and therefore not subject to spurious pickup. Since the resistor is usually 10-1000Ω, typically 50Ω, this is not a serious problem anyway. The disadvantage is that the bias supply is floating. If this is a small battery, it cannot easily be varied. If it is a large electronic supply, the capacitance to ground will be so large that ac signals will be short-circuited to ground, and the probe cannot be expected to have good frequency response. The bias supply can also act as an antenna to pick up spurious signals. To avoid this, one can ground the bias supply and put the measuring resistor on the hot side, as shown in Fig. 12b. This is usually done if the bias supply generates a sweep voltage. However, the voltage across R now has to be measured with a differential amplifier or some other floating device; or, it can be optoelectronically transmitted to a grounded circuit. Commercial hardware can use a floating analog-to-digital converter to record the voltage across R. The probe voltage V_p should be measured on the ground side of R so as not to load the probe with another stray capacitance.

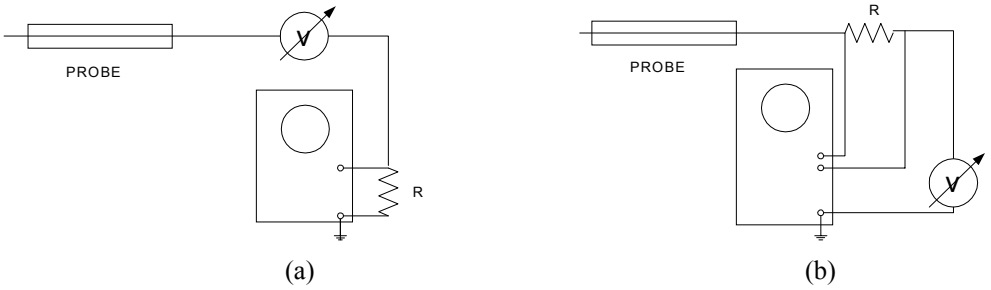

Fig. 12. Two basic configurations for the probe circuit.

To measure plasma potential with a Langmuir probe, one can terminate the probe in a high impedance, such as the 1 MΩ input resistance of the oscilloscope. This is called a *floating probe*. A lower R, like 100K, can be used to suppress pickup. The minimum value of R has to be high enough that the IR drop through it does change the measured voltage. A rough rule of thumb is that $I_{sat}R$ should be much greater than T_{eV}, or $R >> T_{eV}/I_{sat}$, where I_{sat} is the ion saturation current defined above. The voltage measured is not the plasma potential but the floating potential. The large value of R means that good frequency response is difficult to achieve because of the RC time constant of stray capacitances. One can improve the frequency response with *capacitance neutralization* techniques, but even then it is hard to make a floating probe respond to rf frequencies. The rule of thumb quoted above comes from the circuit diagram of Fig. 13, where the load line of the terminating resistor is shown together with the probe characteristic. The line on the left is for a small resistor used to measure current; its slope is nearly vertical, so that the marked intersection with the $I - V$ curve gives the current near the set point V_p. Note that $I_e = -I$ is plotted vertically, so that the load lines have negative slopes. The line at the right represents a large resistor used to measure floating potential. Its intersection with the $I - V$ curve is near V_f. Since the $I - V$ curve varies about I_{sat} over a voltage range of about T_{eV} , its effective impedance there is about T_{eV}/I_{sat}. Very approximately, then, R should be much larger than this value to measure V_f.

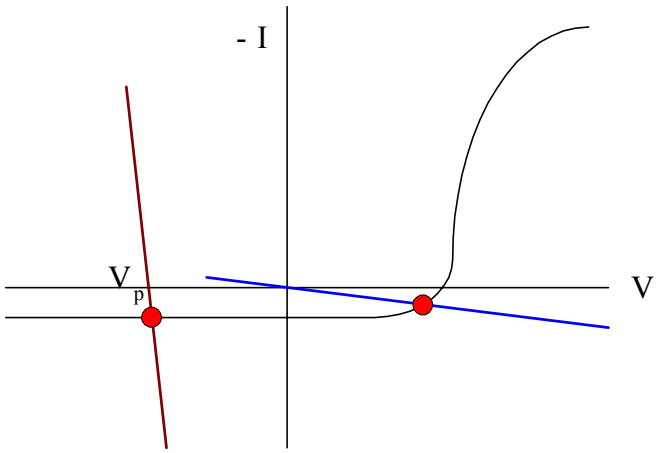

Fig. 13. The operating points of a biased probe and a floating probe.

C. RF compensation

Langmuir probes used in rf plasma sources are subject to rf pickup which can greatly distort the $I - V$ characteristic and give erroneous results. ECR sources which operate in the microwave regime do not have this trouble because the frequency is so high that it is completely decoupled from the circuitry, and the measured currents are the same as in a DC discharge. However, in rf plasmas, the space potential can fluctuate is such a way that the circuitry responds incorrectly. The problem is that the $I - V$ characteristic is nonlinear. The "V" is actually the potential difference V_p - V_s , where V_p is a DC potential applied to the probe, and V_s is a potential that can fluctuate at the rf frequency and its harmonics. If one displaces the $I - V$ curve horizontally back and forth around a center value V_0, the average current I measured will not be $I(V_0)$, since I varies exponentially in the transition region and also changes slope rapidly as it enters the ion and electron saturation regions. The effect of this is to make the $I - V$ curve wider, leading to a falsely high value of T_e and shifting the floating potential V_f to a more negative value. This is illustrated in Figs. 14 and 15.

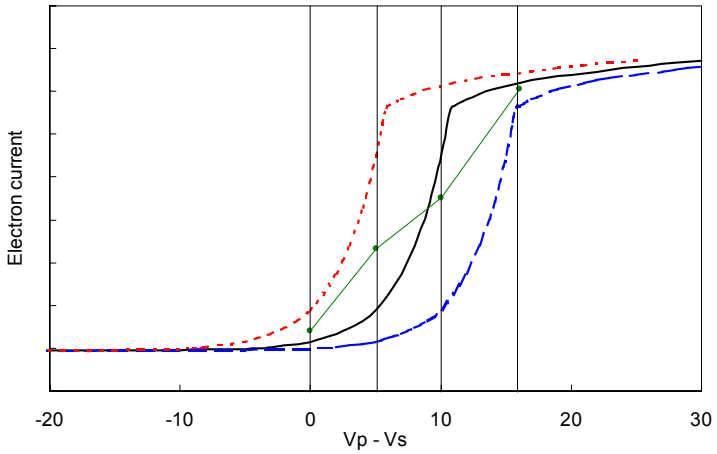

Fig. 14. The center curve is the correct $I - V$ curve. The dashed ones are displaced by ±5V, representing changes in V_s. At the vertical lines, the average I_e between the displaced curves is shown by the dot. The line through the dots is the time-averaged $I - V$ curve that would be observed, differing greatly from the correct curve.

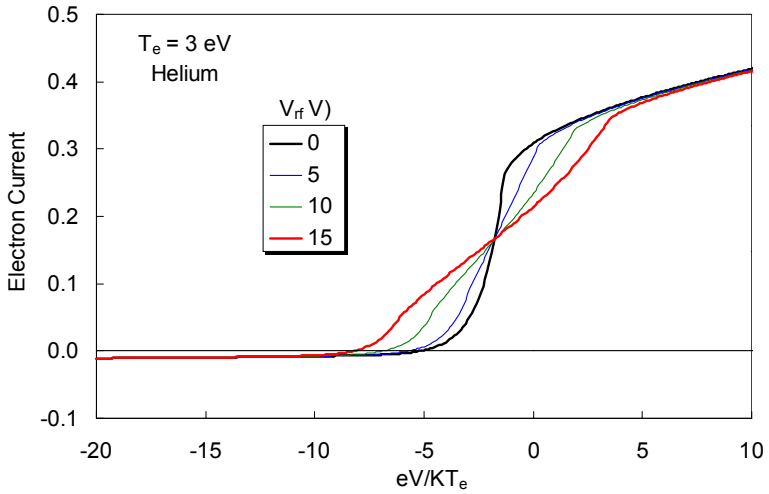

Fig. 15. Computed $I - V$ curves for sinusoidal V_s oscillations of various amplitudes.

Without proper rf compensation, Langmuir probe data in rf discharges can give spurious data on T_e, V_f, and f(v). However, if one needs to find only the plasma density, the probe can be biased so that V never leaves the ion saturation region, which is linear enough that the average I_{sat} will be the correct value.

Several methods for reducing rf effects have been tried. One is to tap off a sinusoidal rf signal from the power supply and mix this with the probe signal with variable phase and amplitude. When the resultant $I - V$ curve gives the lowest value of T_e, one has probably simulated the V_s oscillations. This method has the disadvantage that the V_s oscillations can contain more than one harmonic. A second method is to measure the V_s oscillations with another probe or section of the wall which is floating, and add that signal to the probe current signal with variable phase and amplitude. The problem with this method is that the V_s fluctuations are generally not the same everywhere. A third method is to isolate the probe tip from the rest of the circuit with an rf choke (inductor), so that the probe tip is floating at rf frequencies but is fixed at the DC probe bias at low frequencies. The probe then follows the V_s fluctuations, maintaining the same dc bias between V_p and V_s. The problem is that the probe tip does not draw enough current to fill the stray capacitances that connect it to ground at rf frequencies. One way is to place a large slug of metal inside the insulator between the probe tip and the chokes. This metal slug has a large area and therefore picks up enough charge from the V_s oscillations to drive the probe tip to follow them. However, we have found[7] that the best way is to use an external floating electrode, which could be a few turns of wire around the probe insulator, and connect it through a capacitor to a point between the probe tip and the chokes (Fig. 9). The charge collected by this comparatively large "probe" is then sufficient to drive the probe tip so that V_p - V_s remains constant. In the Hiden probe (Fig. 9), the auxiliary electrode is very large and is ac-coupled to the probe tip through a thin insulating layer. Note that this auxiliary electrode supplies only the rf voltage; the dc part is still supplied by the external power supply. The design of the chokes is also critical: they must have high enough Q to present a resonantly high impedance at both the fundamental and the second harmonic of the rf frequency. This is the reason there are two pairs of chokes in Fig. 9. One pair is resonant at ω, and the other at 2ω. Two chokes are used in series to increase the Q. A compromise has to be made between high Q and small physical size of the chokes. Figure 16 shows an $I - V$ curve taken with and without the auxiliary electrode, showing that the chokes themselves are usually insufficient.

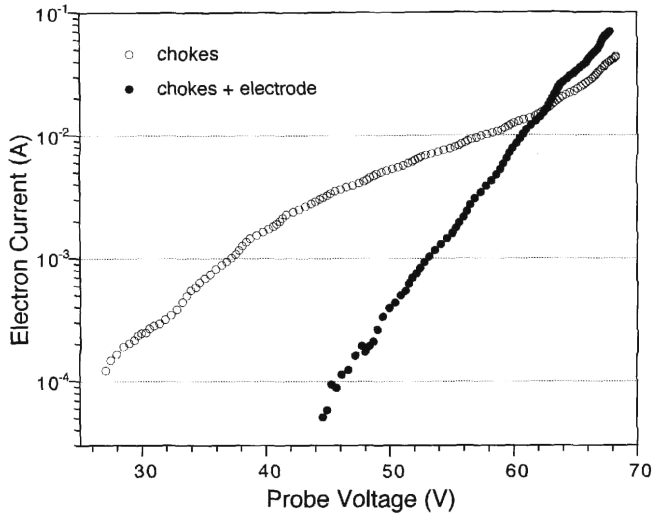

Fig. 16. $I - V$ curves taken with and without an auxiliary electrode.

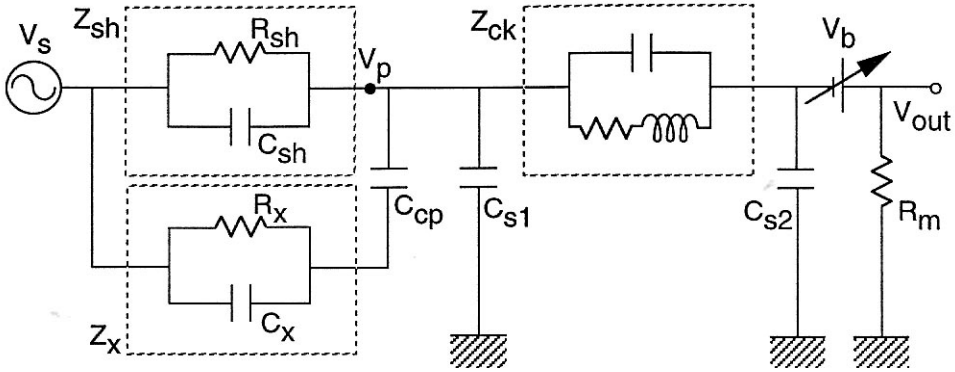

Fig. 17. Circuit diagram of a probe-plasma system with rf compensation.

To calculate how much compensation is necessary, we have to understand the probe-plasma circuit, shown in Fig. 17. The probe tip is coupled to the oscillating space potential $\tilde{V}_{rf}$ through a sheath capacitance $C_{\rm sh}$. The sheath impedance is represented by $R_{\rm sh}$ and $C_{\rm sh}$, and that of the auxiliary electrode by $R_{\rm x}$ and $C_{\rm x}$. The latter is coupled to the probe tip P at $V_{\rm p}$ through a capacitance $C_{\rm cp}$. The impedance of the chokes is $Z_{\rm ck}$, and $C_{\rm s1}$ and $C_{\rm s2}$ are stray capacitances. $V_{\rm b}$ is the bias supply, and $R_{\rm m}$ the current-measuring resistor. By solving Poisson's equation, $C_{\rm sh}$ and $C_{\rm x}$ are are found to be[9, 7]

$$C_{sh,x} = \frac{1}{2^{7/4}} \frac{\varepsilon_0 A_{sh,x}}{\lambda_D} \left[\frac{e(V_s - V_p)}{KT_e} \right]^{-3/4}, \tag{8}$$

where the A's are the respective surface areas. The corresponding impedances $|Z_{\rm sh,x}|$ are $1/\omega C_{\rm sh,x}$. For the probe tip to follow $\tilde{V}_{rf}$, the effective impedance $Z_{\rm eff}$ of the isolating inductors $Z_{\rm ck}$ must be large compared with the larger of $|Z_{\rm sh,x}|$. $Z_{\rm eff}$ is the parallel combination of $Z_{\rm ck}$ and the stray impedance to ground of the short wire between P and the chokes. For instance, a 1 cm long wire has a capacitance to ground of ≈ 0.25 pF, and the stray impedance at 2 MHz is ≈ 330 kΩ. For maximum effectiveness, $Z_{\rm ck}$ should be of this order. RF compensation is effective against fluctuations of order $\tilde{V}_{rf}$ if

$$Z_{eff} >> Z_{sh,x}\left(\frac{e|\tilde{V}_{rf}|}{KT_e}-1\right), \tag{9}$$

so that the rf amplitude leaking through to R_m is much smaller than the characteristic voltage over which the probe current varies; namely, T_{eV}. Figure 18 shows a sample calculation of this criterion for an electrode with A_x = 2 cm^2 and inductors with Z_{ck} = 250 KΩ at 2 MHz. We have taken $|\tilde{V}_{rf}|$ / T_e = 30 and $|V_s - V_p|$ / T_e = 5. This is the region near the floating potential where the nonlinearity of the $I - V$ curve is most severe. It is seen that an unaided probe cannot satisfy Eq.(9), and a 2-cm^2 electrode is required to measure densities down to the mid-10^{10} cm^{-3} range.

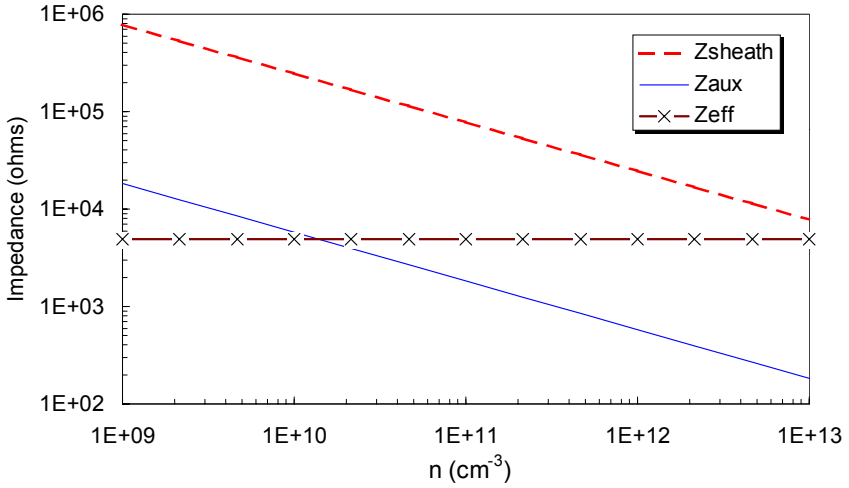

Fig. 18. Example of design curves for an auxiliary electrode.

III. THEORIES OF ION COLLECTION

A. Planar sheaths

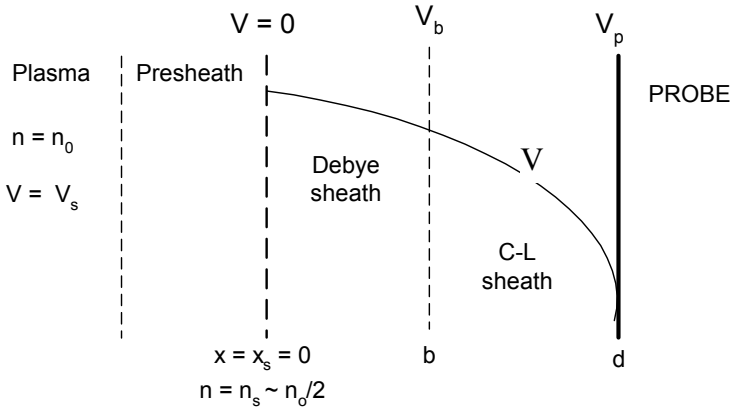

Fig. 19. Structure of the sheath regions at a plane probe (not to scale!).

Though the space potential varies smoothly between the plasma and the probe or wall, it is customarily divided into several regions for convenience. These are shown in Fig. 19. Adjacent to the surface is the Child-Langmuir (CL) sheath, where the electron density n_e is negligible. Next is the Debye sheath, in which the electron density n_e drops exponentially with V. At the sheath edge $x = x_s$ (usually set as the origin), quasineutrality holds, so that $n_e \approx$

n_i. Here the electron distribution is isotropic (except for the few energetic ones that reach the probe), but the ion distribution is unidirectional, since the probe absorbs all the incoming ions. To reach this state, a presheath region must exist, in which a small electric field accelerates the ions to a velocity c_s, giving rise to the Bohm current of Eq. (4). The potential drop corresponding to an energy of $\frac{1}{2}Mc_s^2$ is $\frac{1}{2}KT_e$. Eq. (1) then shows that the density n_s there is $n_s = n_0 \exp(-1/2) = 0.61$, which is closer to 0.5 if the ions are not completely cold. The Debye sheath is usually thicker than the CL sheath, and the presheath is much thicker than both. Its length is scaled to the collision mean free path or ionization length. Finally, at the extreme left, the presheath joins on to the main plasma, which is neutral and ideally has no electric field.

The exact solution for a combined Debye-CL sheath in plane geometry can be derived from Poisson's equation

$$\frac{d^2V}{dx^2} = \frac{e}{\varepsilon_0}(n_e - n_i)\,. \tag{10}$$

In a strictly 1-D problem, we must assume a sheath edge, since if the ion velocity v_i were zero at infinity, the density there would have to be infinite for the ion flux to be finite. We therefore choose $x = 0$ to be at x_s, where the Bohm formula holds, and define $V = 0$ there. For Maxwellian electrons, we have everywhere

$$n_e = n_s e^{eV/KT_e} = n_s e^{-\eta}, \qquad \eta \equiv -eV/KT_e\,. \tag{11}$$

For the ions, energy conservation requires

$$\tfrac{1}{2}Mv_i^2 = \tfrac{1}{2}Mc_s^2 - eV, \qquad v_i = \left(c_s^2 - 2eV/M\right)^{1/2}. \tag{12}$$

Continuity of ion flux then gives

$$n_i v_i = n_s c_s\,, \qquad n_i = n_s \frac{c_s}{v_i} = n_s\left(1 - \frac{2eV}{Mc_s^2}\right)^{-1/2} = n_s\left(1+2\eta\right)^{-1/2} \tag{13}$$

Eq. (10) then becomes

$$\frac{d^2V}{dx^2} = \frac{e}{\varepsilon_0} n_s\left[e^{-\eta} - \left(1+2\eta\right)^{-1/2}\right] = -\frac{KT_e}{e}\frac{d^2\eta}{dx^2} \tag{14}$$

Normalization to the Debye length λ_{Ds} at the sheath edge yields

$$\eta'' = \left[\left(1+2\eta\right)^{-1/2} - e^{-\eta}\right], \tag{15}$$

where the ($'$) indicates derivative with respect to $\xi \equiv x/\lambda_{Ds}$. Following standard procedure, we multiply by an integration factor η' and integrate from $\eta = 0$ to η. Setting $\eta' = 0$ at $\xi = 0$, we obtain

$$\eta' = \sqrt{2}\left[(1+2\eta)^{1/2} + e^{-\eta} - 2\right]^{1/2}. \tag{16}.$$

The next integration has to be done numerically, and the result is shown in Fig. 20 for two assumed values of $\eta''(0)$. The "sheath thickness" is indeterminate because it depends on the

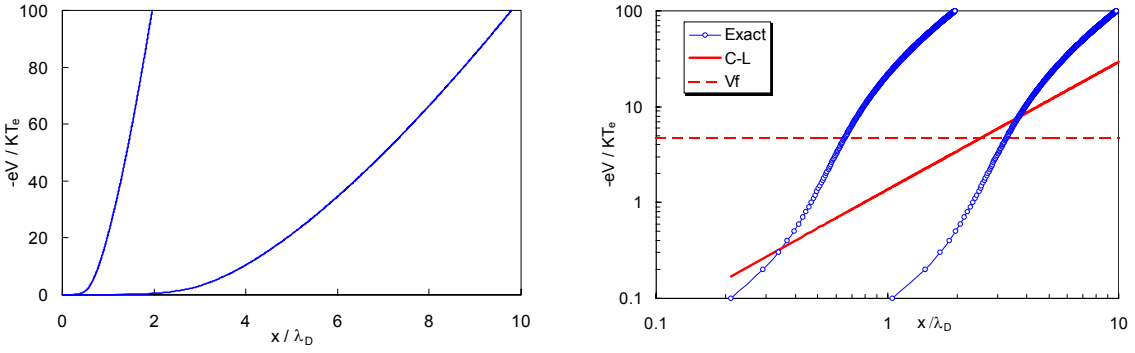

(a) (b)

Fig. 20. Numerical solution of the plane sheath problem for two different initial values of V' on (a) linear and (b) logarithmic scales. The dashed line in (b) is the floating potential, and a floating probe would be located at its intersection with the $V(x)$ curve. The solid line in (b) is the slope predicted by the CL law; it is not followed until x is much larger.

assumed boundary condition at $\xi = 0$. If $\eta' = 0$ there, then η'' or another derivative must be given a finite value in order for the curve to rise above zero. In reality, the boundary condition on η' and η'' is determined by matching to the presheath. The two curves of Fig. 20a are plotted logarithmically in Fig. 20b. Once η becomes appreciable, the curve $\eta(\xi)$ has a definite shape, but its position relative to the sheath edge cannot be found without a presheath calculation, which is not only difficult but also depends on the details of the discharge. Thus, a plane sheath does not have a unique thickness. The sheath edge conditions are artificially chosen to simplify the problem to make it tractable, and these control the sheath thickness. There is currently a dispute in the literature[10,11,12,13] as to where the sheath edge should be chosen and whether or not a valid matching condition to the presheath is possible. In any case, there is no useful solution of the plane probe problem without assuming a sheath edge, and the matching condition there affects only the position of the sheath edge on a presheath length scale.

As far as saturation ion currents to a plane probe are concerned, there is strictly no collisionless theory possible. An infinitely large probe collects all the ions created. A section of it would collect the Bohm current with a coefficient α representing the density at the sheath edge. This density depends on the geometry of the surface where the ions come from, and this surface may not be planar.

B. Orbital Motion Limit (OML) theory

As the negative bias on a probe is increased to draw I_i, the sheath on cylindrical and spherical probes expands, and I_i does not saturate. Fortunately, the sheath fields fall off rapidly away from the probe so that exact solutions for $I_i(V_p)$ can be found. We consider cylindrical probes here because spherical ones are impractical to make, though the theory for them converges better. The simplest theory is the orbital-motion-limited (OML) theory of Langmuir and associates[14].

Consider ions coming to the attracting probe from infinity in one direction with velocity v_0 and various impact parameters p. The plasma potential V is 0 at ∞ and is negative everywhere, varying gently toward the negative probe potential V_p . Conservation of energy and angular momentum give

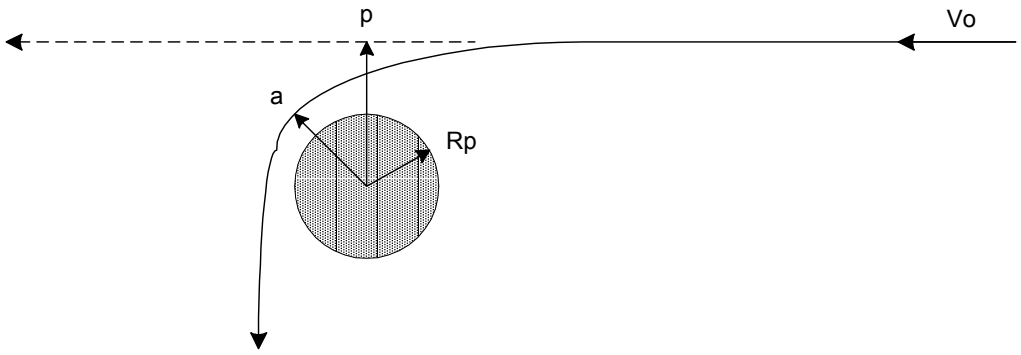

Fig. 21

$$\begin{aligned} &½\, mv_0^2 = ½\, mv_a^2 + eV_a \equiv -eV_0 \\ &pv_0 = av_a \end{aligned} \tag{17}$$

where $eV < 0$ and a is the distance of closest approach to the probe of radius R_p . Solving, we obtain

$$½mv_a^2 = ½mv_0^2\left(1+\frac{V_a}{V_0}\right), \qquad p = a\frac{v_a}{v_0} = a\left(1+\frac{V_a}{V_0}\right)^{1/2}. \tag{18}$$

If $a \le R_p$, the ion is collected; thus, the *effective* probe radius is $p(R_p)$. For monoenergetic particles, the flux to a probe of length L is therefore

$$\Gamma = 2\pi R_p L(1+V_a/V_0)^{1/2}\Gamma_r\,, \tag{19}$$

where Γ_r is the random flux of ions of that energy. Langmuir then extended this result to energy distributions which were Maxwellian at some large distance $r = s$ from the probe, where s is the "sheath edge". The random flux Γ_r is then given by the usual formula

$$\Gamma_r = n\left(\frac{KT_i}{2\pi M}\right)^{1/2}. \tag{20}$$

With A_p defined as the probe area, integrating over all velocities yields the cumbersome expression

$$\Gamma = A_p\Gamma_r\left\{\frac{s}{a}\mathrm{erf}(\Phi^{½}) + e^{\chi}[1-\mathrm{erf}(\chi+\Phi)^{½}]\right\}, \tag{21}$$

$$\text{where } \chi \equiv -eV_p/KT_i, \quad \Phi \equiv \left(\frac{a^2}{s^2-a^2}\right)\chi, \quad a = R_p\,.$$

Fortunately, there are small factors. In the limit $s >> a$, when OML theory applies, if at all, we have $\Phi << \chi$, and for $T_i \to 0$, $1/\chi << 1$. Expanding in Taylor series, we find that the T_i dependences of χ and Γ_r cancel, and a finite limiting value of the OML current exists, independently of the value of T_i.

$$I \xrightarrow[T_i\to 0]{} A_p ne\frac{\sqrt{2}}{\pi}\left(\frac{|eV_p|}{M}\right)^{1/2}. \tag{22}$$

Thus, the OML current is proportional to $|V_p|^{1/2}$, and the $I - V$ curve is a parabola, while the $I^2 - V$ curve is a straight line. This scaling is the result of conservation of energy and angular momentum. Because ions have large angular momentum at large distances, though they have small velocities, they tend to orbit the probe and miss it. The probe voltage draws them in. The value of T_i cancels out mathematically, but T_i has to be finite for this physical mechanism to work.

The OML result, though simple, is very restricted in applicability. Since the sheath radius s was taken to be infinite, the density has to be so low that the sheath is much larger than the probe. The potential variation V(r) has to be gentle enough that there does not exist an "absorption radius" inside of which the E-field is so strong that no ions can escape being collected. Except in very tenuous plasmas, a well developed sheath and an absorption radius exist, and OML theory should be invalid, though it may give good results outside of its intended range. At higher densities, the $I^2 - V$ dependence of I_{sat} is often observed and is mistakenly taken as evidence of orbital motion in a regime where OML cannot apply.

An Excel program for analyzing an $I - V$ curve using OML theory is available on the author's website[15] under Presentations.

C. Allen-Boyd-Reynolds (ABR) theory

To do a proper sheath theory, one has to solve Poisson's equation for the potential $V(r)$ everywhere from the probe surface to $r = \infty$. Allen, Boyd, and Reynolds[16] (ABR) simplified the problem by assuming *ab initio* that $T_i = 0$, so that there are no orbital motions at all: the ions are all drawn radially into the probe. Originally, the ABR theory was only for spherical probes, but it was later extended to cylindrical probes by Chen[17], as follows. Assume that the probe is centered at $r = 0$ and that the ions start at rest from $r = \infty$, where $V = 0$. Poisson's equation in cylindrical coordinates is

$$\frac{1}{r}\frac{\partial}{\partial r}\left(r\frac{\partial V}{\partial r}\right) = \frac{e}{\varepsilon_0}\left(n_e - n_i\right), \qquad n_e = n_0 e^{eV/KT_e}. \tag{17}$$

To electrons are assumed to be Maxwellian. To find n_i, let I be the total ion flux per unit length collected by the probe. By current continuity, the flux per unit length at any radius r is

$$\Gamma = n_i v_i = I/2\pi r, \quad \text{where} \quad v_i = \left(-2eV/M\right)^{1/2}. \tag{18}$$

Thus,
$$n_i = \frac{\Gamma}{v_i} = \frac{I}{2\pi r}\left(\frac{-2eV}{M}\right)^{-1/2}. \tag{19}$$

Poisson's equation can then be written

$$\frac{1}{r}\frac{\partial}{\partial r}\left(r\frac{\partial V}{\partial r}\right) = -\frac{e}{\varepsilon_0}\left[\frac{I}{2\pi r}\left(\frac{-2eV}{M}\right)^{-1/2} - n_0 e^{eV/KT_e}\right] \tag{20}$$

Defining

$$\eta \equiv -\frac{eV}{KT_e}, \qquad c_s \equiv \left(\frac{KT_e}{M}\right)^{1/2}, \tag{21}$$

we can write this as

$$\frac{KT_e}{e}\frac{1}{r}\frac{\partial}{\partial r}\left(r\frac{\partial \eta}{\partial r}\right) = -\frac{e}{\varepsilon_0}\left[\frac{I}{2\pi r}\frac{(2\eta)^{-1/2}}{c_s} - n_0 e^{-\eta}\right]. \tag{22}$$

or

$$-\frac{\varepsilon_0 KT_e}{n_0 e^2}\frac{1}{r}\frac{\partial}{\partial r}\left(r\frac{\partial \eta}{\partial r}\right) = \frac{I}{2\pi r}\frac{(2\eta)^{-1/2}}{n_0 c_s} - e^{-\eta}. \tag{23}$$

The Debye length appears on the left-hand side as the natural length for this equation. We therefore normalize r to λ_D by defining a new variable ξ:

$$\xi \equiv \frac{r}{\lambda_D}, \qquad \lambda_D \equiv \left(\frac{\varepsilon_0 KT_e}{n_0 e^2}\right)^{1/2}. \tag{24}$$

Eq. (23) now becomes

$$\begin{aligned}
\frac{\partial}{\partial \xi}\left(\xi\frac{\partial \eta}{\partial \xi}\right) &= \frac{I\xi}{2\pi r}\frac{1}{n_0 c_s}(2\eta)^{-1/2} - \xi e^{-\eta} \\
&= \frac{I}{2\pi n_0}\frac{1}{\lambda_D c_s}(2\eta)^{-1/2} - \xi e^{-\eta} \\
&= \frac{I}{2\pi n_0}\left(\frac{n_0 e^2}{\varepsilon_0 KT_e}\frac{M}{KT_e}\right)^{1/2}(2\eta)^{-1/2} - \xi e^{-\eta} \\
&= \frac{eI}{2\pi KT_e}\left(\frac{M}{2\varepsilon_0 n_0}\right)^{1/2}\eta^{-1/2} - \xi e^{-\eta}
\end{aligned} \tag{25}$$

Defining

$$J \equiv \frac{eI}{2\pi KT_e}\left(\frac{M}{2\varepsilon_0 n_0}\right)^{1/2}, \tag{26}$$

we arrive at the ABR equation for cylindrical probes:

$$\frac{\partial}{\partial \xi}\left(\xi\frac{\partial \eta}{\partial \xi}\right) = J\eta^{-1/2} - \xi e^{-\eta}. \tag{27}$$

For each assumed value of J (normalized probe current), this equation can be integrated from $\xi = \infty$ to any arbitrarily small ξ. The point on the curve where $\xi = \xi_p$ (the probe radius) gives the probe potential η_p for that value of J. By computing a family of curves for different J (Fig. 22), one can obtain a $J - \eta_p$ curve for a probe of radius ξ_p by cross-plotting (Fig 23). Of course, both J and ξ_p depend on the unknown density n_0, which one is trying to determine from the measured current I_i. (KT_e is supposed to be known from the electron characteristic.) The extraction of n_0 from these universal curves is a trivial matter for a computer. In the graphs the quantity $J\xi_p$ is plotted, since that is independent of n_0. Note that for

small values of ξ_p, I^2 varies linearly with V_p, as in OML theory, but this agreement is accidental[18], since there is no orbiting here.

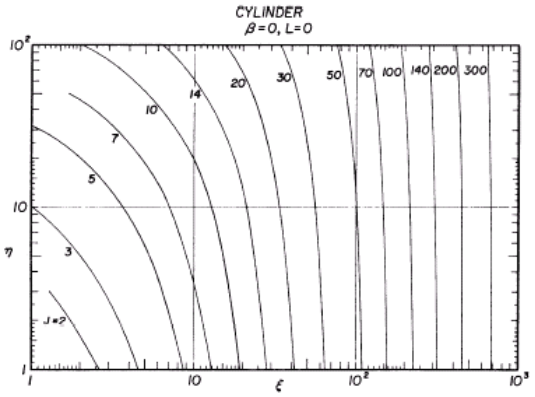

Fig. 22. ABR curves for $\eta(\xi)$.

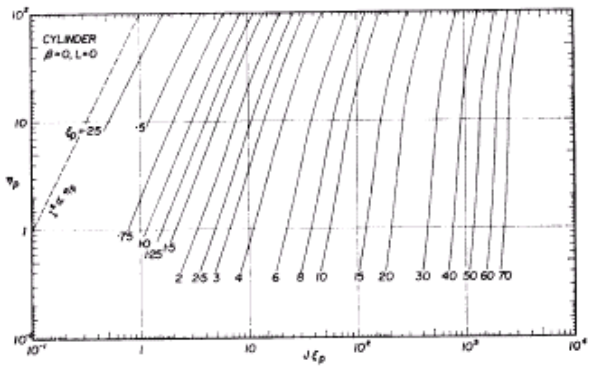

Fig. 23. V–I curves derived from $\eta(\xi)$.

An Excel program for analyzing an $I - V$ curve using ABR theory is available on the author's website[15] under Presentations.

D. Bernstein-Rabinowitz-Laframboise (BRL) theory

The first probe theory which accounted for both sheath formation and orbital motions was published by Bernstein and Rabinowitz[19] (BR), who assumed an isotropic distribution of ions of a single energy E_i. This was further refined by Laframboise[20] (L), who extended the calculations to a Maxwellian ion distribution at temperature T_i. The BRL treatment is considerably more complicated than the ABR theory. In ABR, all ions strike the probe, so the flux at any radius depends on the conditions at infinity, regardless of the probe radius.

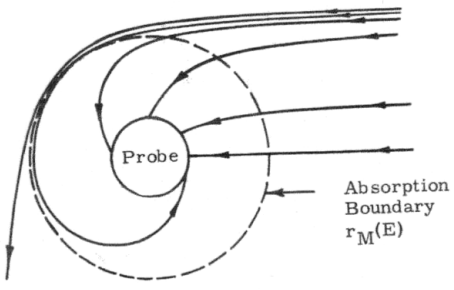

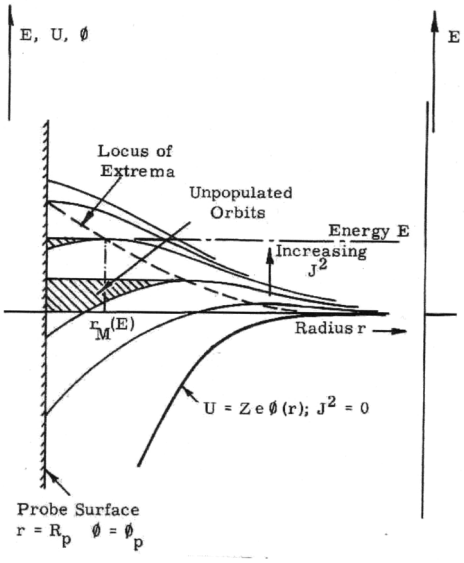

Fig. 24. Definition of absorption radius. Fig. 25. Effective potential seen by ions with angular momentum J.

That is why there is a set of universal curves. In BRL theory, however, the probe radius must be specified beforehand, since those ions that orbit the probe will contribute twice to the ion density at any given radius r, while those that are collected contribute only once. The ion density must be known before Poisson's equation can be solved, and clearly this depends on the presence of the probe. There is an "absorption radius" (Fig. 24), depending on J, inside

of which all ions are collected. Bernstein solved the problem by expressing the ion distribution in terms of energy E and angular momentum J instead of v_r and $v_\perp$. Ions with a given J see an effective potential barrier between them and the probe. They must have enough energy to surmount this barrier before they can be collected. In Fig. 25, the lowest curve is for ions with $J = 0$; these simply fall into the probe. Ions with finite J see a potential hill. With sufficient energy, they can climb the hill and fall to the probe on the other side. The dashed line through the maxima shows the absorption radius for various values of J. For cylindrical probes, BRL requires the solution of the equation

$$\begin{aligned} \frac{1}{\xi}\frac{d}{d\xi}\left(\xi\frac{d\eta}{d\xi}\right) &= 1-\frac{1}{\pi}\sin^{-1}\left(\frac{\iota/\xi^2}{1+\eta/\beta}\right)^{1/2} \quad \text{for} \quad \xi>\xi_0 \\ &= \frac{1}{\pi}\sin^{-1}\left(\frac{\iota/\xi^2}{1+\eta/\beta}\right)^{1/2} \quad \text{for} \quad \xi<\xi_0 \end{aligned} \tag{23}$$

where β is the ion energy over KT_e, ι (iota) is a dimensionless probe current per unit length, and the other symbols are as in the ABR theory. The absorption radius ξ_0 occurs there the argument of $\sin^{-1}$ is unity.

For convergence at ∞, the computation tricky and tedious, more so when the ions have an energy spread. It turns out that KT_i makes little difference if $T_i/T_e < 0.1$ or so, as it usually is. Laframboise's extension to a Maxwellian ion distribution is not normally necessary; nonetheless, Laframboise gives the most complete results. Fig. 26 shows an example of ion saturation curves from the BRL theory. One sees that for large probes ($R_p/\lambda_D >>1$) the ion current saturates well, since the sheath is thin. For small R_p/λ_D, I_i grows with increasing V_p as the sheath radius increases.

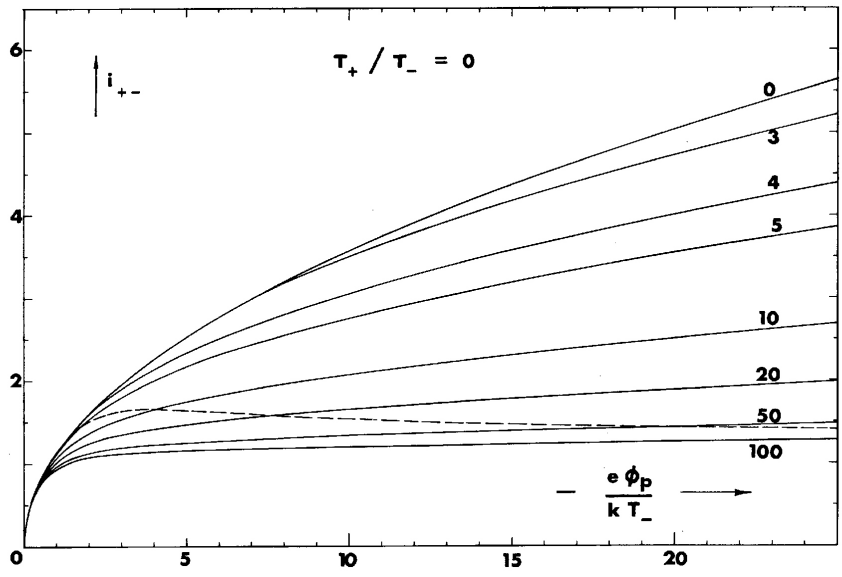

Fig. 26. Laframboise curves for $I_i - V$ characteristics in dimensionless units, in the limit of cold ions. Each curve is for a different ratio R_p/λ_D.

One might think that the ABR result would be recovered if takes $T_i = 0$ or $E_i = 0$ in the BRL computation. However, this happens only for spherical probes. For cylindrical probes, there is a problem of nonuniform convergence. Since the angular momentum is Mvr,

for $r \to \infty$ ions with zero thermal velocity have $J = (M)(0)(\infty)$, an indeterminate form. The correct treatment is to calculate the probe current for $T_i > 0$ and *then* take the limit $T_i \to 0$, as BRL have done. The BRL predictions have been borne out in experiments in fully ionized plasmas[21], but not in partially ionized ones.

An Excel program for analyzing an $I - V$ curve using BRL theory is available on the author's website[15] under Presentations.

E. Parametrized ion curves

Since the ABR theory requires solution of a differential equation and the BRL theory involves such delicate computations that only a programming expert could do, these theories are not easily applied to experimental measurements. However, it is possible to reduce the computed curves to algebraic form by fitting them to simple functions. This has been done by Chen[9]. The Laframboise results are given in graphs such as that in Fig. 26. The probe voltage is normalized to KT_e, which is determined from the transition region, and the ion current is normalized to the Bohm current, which depends on KT_e and the density n. There is one curve for each value of ξ_p (or ξ) = R_p/λ_D. If ξ_p is known, one can find the curve on which the experimental points lie by varying n, and thus n can be determined. Of course, λ_D and thus ξ_p also depends on n, but the iteration to find n can easily be done by a computer. But first the graphical curves of Fig. 26 have to be parametrized to facilitate interpolation between available values. The following definitions will be needed to convert the results into laboratory units:

$$\eta \equiv -\frac{e(V_p - V_s)}{KT_e} \qquad J = \frac{I_i}{2\pi e R_p L}\frac{1}{n}\left(\frac{KT_e}{2\pi M}\right)^{-1/2} \tag{24}$$

$$\xi \equiv R_p / \lambda_D$$

The Laframboise curves can be fitted with the following function:

$$\frac{1}{J^4} = \frac{1}{(A\eta^B)^4} + \frac{1}{(C\eta^D)^4}. \tag{25}$$

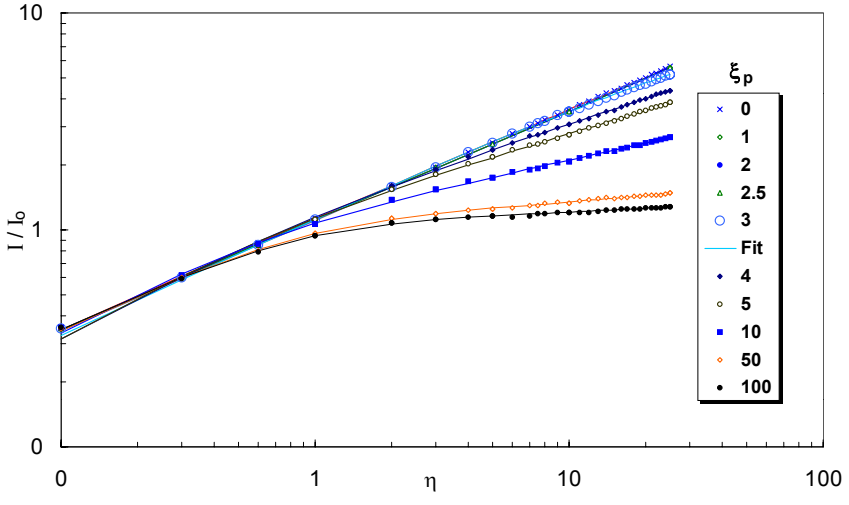

Fig. 27. Analytic fits (lines) to computed data (points) by Laframboise.

Figure 27 shows the fit for available values of ξ_p on a log-log scale. Note that the curves approach the OML limit $I^2 \propto V$ as either ξ_p or η gets small. The parameters A,B,C, and D depend on the value of ξ_p (abbreviated as ξ) as shown in Fig. 28. They do not vary smoothly,

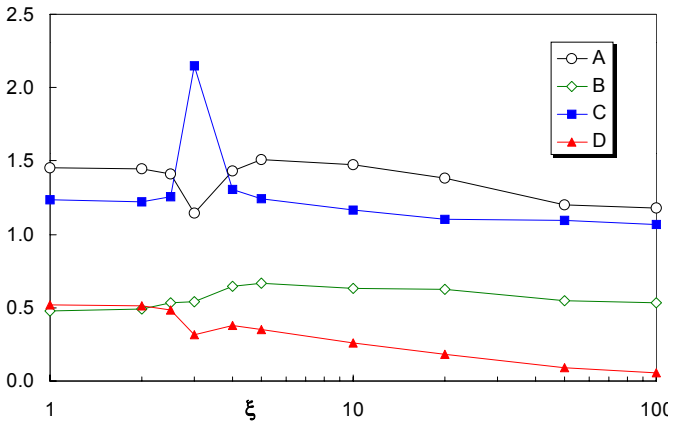

Fig. 28. Behavior of the parameters A,B,C, and D with ξ.

and to find an analytic fit we had to somewhat degrade the fits on Fig. 27. The result is

$$A = a + \frac{1}{\frac{1}{b\xi^c} - \frac{1}{d\ln(\xi/f)}}$$
$$B, D = a + b\xi^c \exp(-d\xi^f) \qquad (26)$$
$$C = a + b\xi^{-c}$$

where the coefficients a to f are given by

Table 1: Coefficients for computing BRL curves

	a	b	c	d	f
A	1.12	.00034	6.87	0.145	110
B	0.50	0.008	1.50	0.180	0.80
C	1.07	0.95	1.01	—	—
D	0.05	1.54	0.30	1.135	0.370

With these fits, the BRL theory can be applied to experimental data. The fits are good to ±5%, which is sufficient, since obtaining n to within 10% with probes is not always possible. One reason is simply that the probe tip changes its area due to sputtering.

The curves of Figs. 22 and 23 for the ABR theory can similarly be parametrized. Eq. (25) can still be used, but Eq. (26) can be replaced by simpler functions:

$$A, C = a\xi^b + c\xi^d$$
$$B, D = a + b\ln\xi + c(\ln\xi)^2 \qquad (27)$$

The values of coefficients a to d are given by

Table 2: Coefficients for computing ABR curves

	a	b	c	d
A	0.864	1.500	0.269	2.050
B	0.479	-0.030	-0.010	—
C	1.008	1.700	0.336	2.050
D	0.384	-0.150	0.013	—

F. Tests of collisionless theories

1. Fully ionized plasmas

The first test of the BRL theory was done in a Q-machine, a fully ionized potassium plasma at 2300K, by Chen et al.[21]. Though there was a strong magnetic field, the ion Larmor radii were large enough that the ion current was not affected by it. Both cylindrical and spherical probes were used. Figure 29 shows that the slope of I_{sat} agrees will with BRL theory. The density was measured independently by microwaves and plasma oscillations, and it was compared with n calculated from I_{sat}. Figure 30 shows that the agreement over two orders of magnitude was within 10%, as long as I_{sat} was taken at $\eta = 20$.

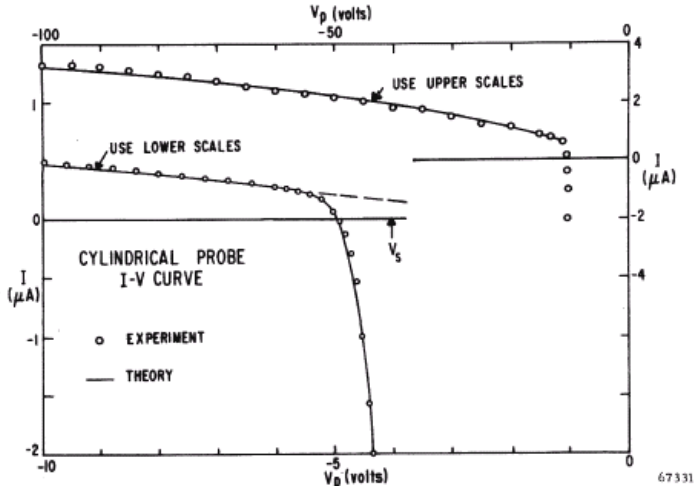

Fig. 29. Saturation ion currents in a potassium Q-machine [Ref. 22].

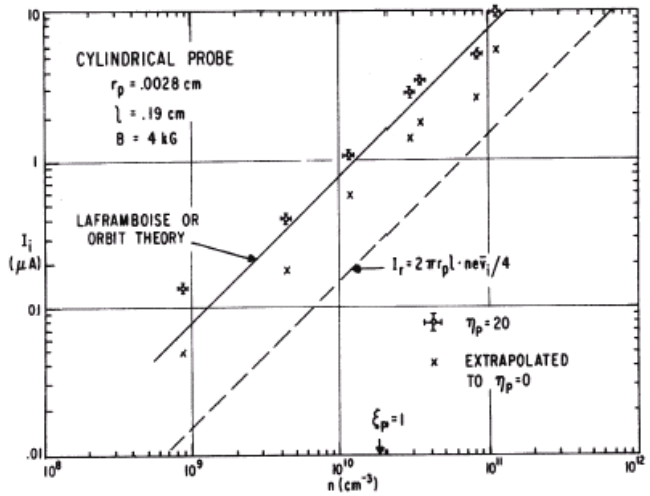

Fig. 30 Variation of I_{sat} with n as compared with BRL theory.

2. High density rf plasmas

The situation is entirely different in partially ionized rf plasmas. In Fig. 31, four probe curves were obtained in rf discharges of different density; i.e., different ξ_p. Each was analyzed using OML, BRL, and ABR theory. The "Hiden" density was obtained automatically by software using OML theory and differs from the "OML" density only in the estimate of KT_e. One sees that the ABR theory gives too low a density, and the BRL theory too high a density, except at low densities, where BRL converges to OML, as it should. Figure 32 shows that I^2 varies linearly with V_p at high density, and both OML and ABR agree with this slope, though different n has to be assumed. The BRL theory, however, predicts a more saturated curve. Comparison between theories is shown clearly in Fig. 33. in which n is varied by increasing the discharge power. It is seen that BRL predicts too high a density, and ABR too low a density, and the disagreement can be larger than a factor 3. Fortuitously, the geometric mean seems to agree with the correct density, as measured with microwaves.

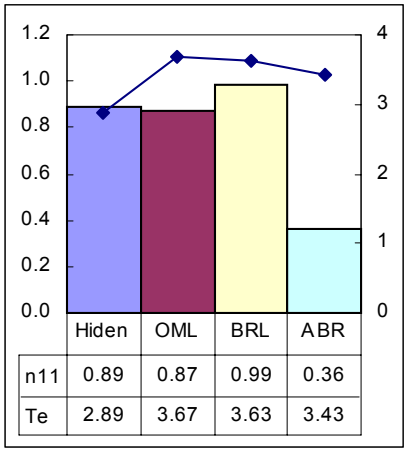

Fig. 15a: $\xi = 1.1$

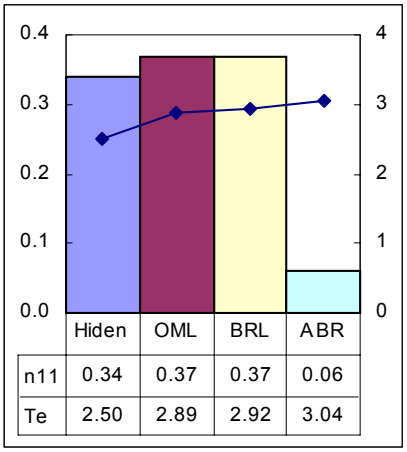

Fig. 15b: $\xi = 3.1$

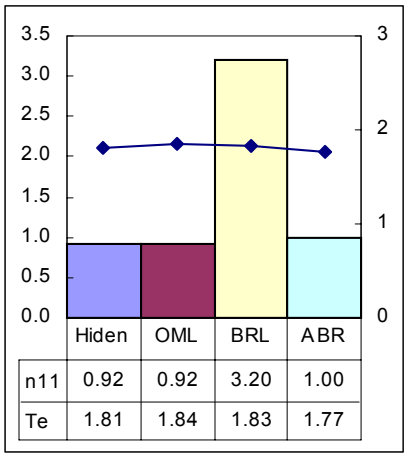

Fig. 15c: $\xi = 4.6$

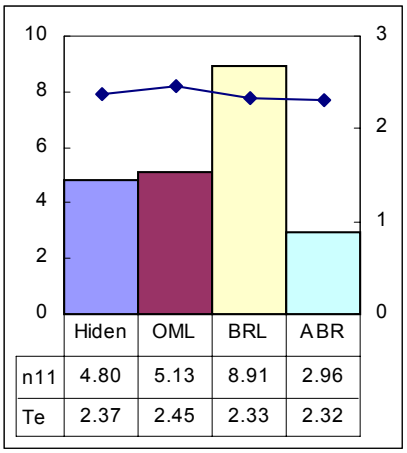

Fig. 15d: $\xi = 9.1$

Fig. 31. Densities (bars, left scale) and T_e's (points, right scale) obtained with various theories from the same probe curves in four discharges with varying ξ_p [Ref. 9].

It is reasonable for the ABR theory to give too low a value of n, since it does not account for orbiting, and thus the expected current is larger than that measured. The lower measured I_{sat} then yields a low value of n. The BRL theory, on the other hand, includes orbiting from ions that have angular momentum far from the probe and predicts a low I_{sat}. A

few charge-exchange collisions, even in the presheath, would destroy this angular momentum and increase the collected current above what is predicted; thus, the BRL theory yield too high a value of density from the measured I_{sat}.

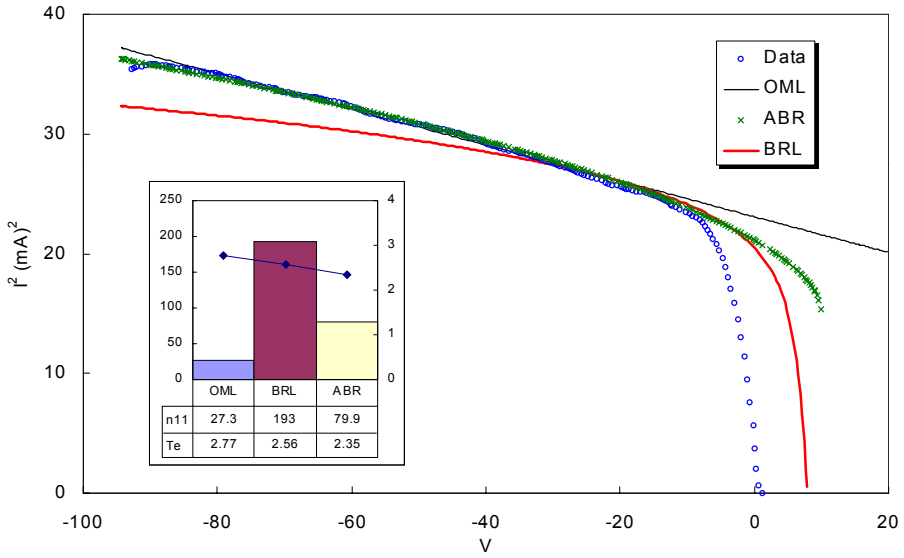

Fig. 32. Comparison of the slopes of the $I^2 - V$ curve from various theories with data from a high-density ($n \approx 10^{13}$ cm^{-3} helicon plasma with $\xi_p \approx 56$.

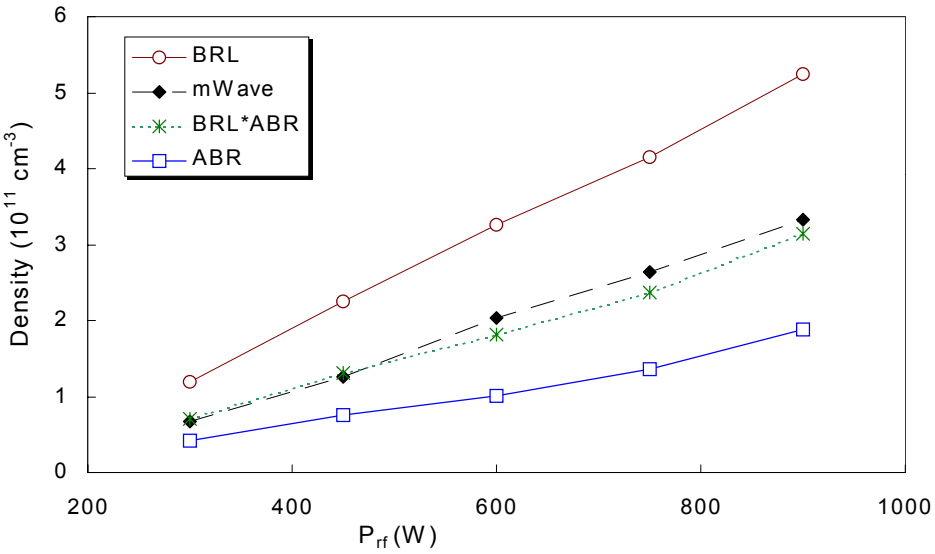

Fig. 33. Comparison of ABR and BRL densities with n measured by microwave interferometry. The dashed line is the geometric mean between the ABR and BRL densities [Ref. 9].

3. Low density dc plasmas`

Recent work by Sternovsky, Robertson, and Lampe[22,23] has evaluated the effect of these collisions. The theory starts with the OML theory, valid for very low densities. Since the ions' temperature T_i is close to the temperature of the neutrals. a collision far from the sheath does not change the ion distribution appreciably, and therefore does not affect the OML current originating there. A collision in the strong-field region, however, replaces an accelerated ion with a thermal ion, which has a much greater probability of being dragged into the probe rather than orbiting it. This gives rise to an additional "charge-exchange

current" I_{cx}. To compute I_{cx} requires knowing the potential distribution $V(r)$. The Poisson equation which determines this is nonlinear, since n_e depends exponentially on $V(r)$, but it is greatly simplified by the fact that n_i is constant regardless of the shape of $V(r)$, a consequence of Liouville's theorem in cylindrical geometry. The net ion current $I_{i,net}$ is then the sum of I_{cx} and the normal OML current. An experimental test is shown in Fig. 34a. Note that the

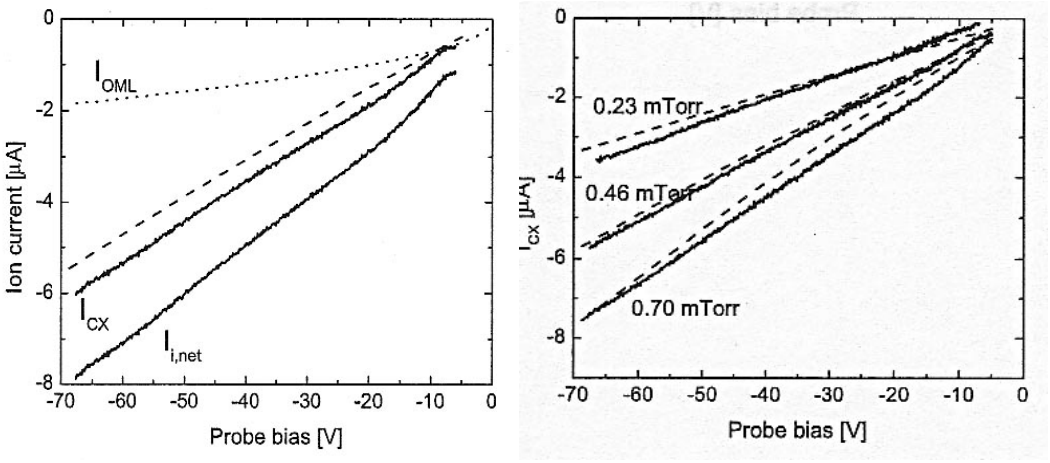

(a) (b)

Fig. 34. (a) The bottom curve is the measured I_{sat}, and the curve I_{cx} is the charge-exchange part of it deduced by subtracting I_{OML} [Eq. (22)]. The dashed line is the computed I_{cx} [Ref. 22]. (b) Agreement at various pressures at a constant density of 1.4×10^7 cm^{-3} .

collisions have caused the ion current to increase linearly, as observed, rather than saturating. The theory was further checked by Sternovsky et al.[22] by comparing I_{cx} with theory at different pressures and with different probe radii R_p. The results for $R_p = 0.19$ mm are shown in Fig. 34b, with very good agreement. At these low values of ξ_p, I_{cx} removes ions from the OML current, but these ions would mostly have orbited the probe anyway, so that the OML curve in Fig. 34a needs no correction. At higher values of ξ_p, however, the sheath is not thick compared with R_p, so that many of the ions contributing to I_{cx} would have been part of I_i, and therefore the OML contribution to $I_{i,net}$ needs to be decreased. This correction was made in a second paper by the same authors[23].

4. Moderate density rf plasmas

At densities typical of ICPs ($10^{10\text{-}12}$ cm^{-3}), I_{sat} behaves neither like the OML current nor the charge-exchange current. On a plot of I^p vs. V_p, where p is an arbitrary exponent, the best fit is obtained with $p = 4/3$, rather than 2 (I_{OML}) or 1 (I_{cx}). An example is shown in Fig. 35. The value 4/3 is reminiscent of the Child-Langmuir law for space-charge-limited emission[24]:

$$J = \frac{4}{9}\left(\frac{2e}{M}\right)^{1/2} \frac{\varepsilon_0 V^{3/2}}{d^2}. \tag{28}$$

For constant current density J, the sheath thickness d should vary as $V^{3/2}$. This suggests setting J equal to the Bohm current density $\alpha_0 n e c_s$ [Eq. (4)] and setting $V = V_f$ to find the sheath thickness d at V_f. From that, the density can be computed from the ion current measured at V_f. This FP method[25] is illustrated in Fig. 36. In cases where the $I_i^{4/3}$–V curve fits a straight

line, extrapolation of this line to where $I_{tot} = 0$ gives the ion contribution at V_f. Eq. (28) can then be solved for d, using the definition of λ_D and $\eta_f = |V_f / T_{eV}|$, obtaining

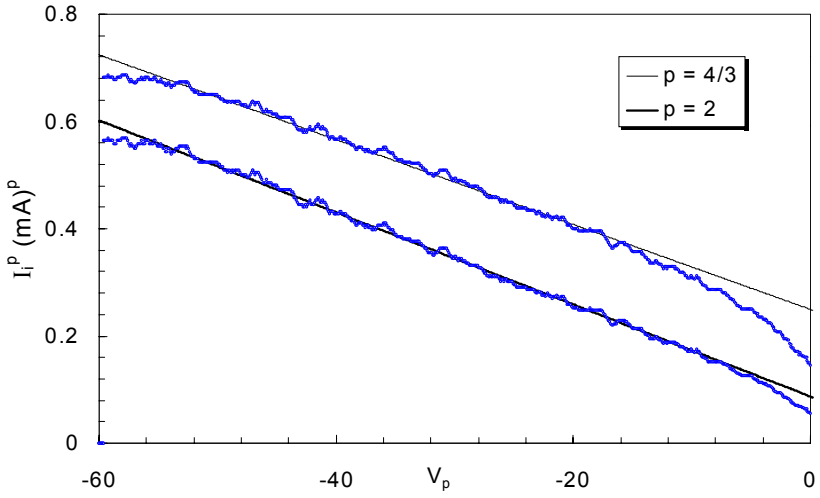

Fig. 35. I^p– V curve for I_{sat} in an rf discharge showing that $p = 4/3$ gives a better fit than p = 2.

$$d = \frac{1}{3}\sqrt{\frac{2}{\alpha_0}}(2\eta_f)^{3/4}\lambda_D \approx 1.0\,\eta_f{}^{3/4}\lambda_D \tag{29}$$

Since the Bohm current is collected at a radius $R_p + d$, the density for a cylindrical probe of length L can be calculated from the formula

$$n = I_i(V_f)/2\pi(R_p + d)eL\alpha_0 c_s\,. \tag{30}$$

Eq. (29) also contains n in λ_D, but Eqs. (29) and (30) reduce to a simple quadratic equation for n which gives surprisingly accurate results[25]. Figures 37 shows the densities this method gives compared with n measured with microwaves. Also shown are the values given by the ABR theory and the electron saturation current from the same data. The FP method yields good results down to about 2 mTorr in argon; below that, the agreement is not as good. This is not surprising, since the FP method should not work at all! The CL formula is for plane

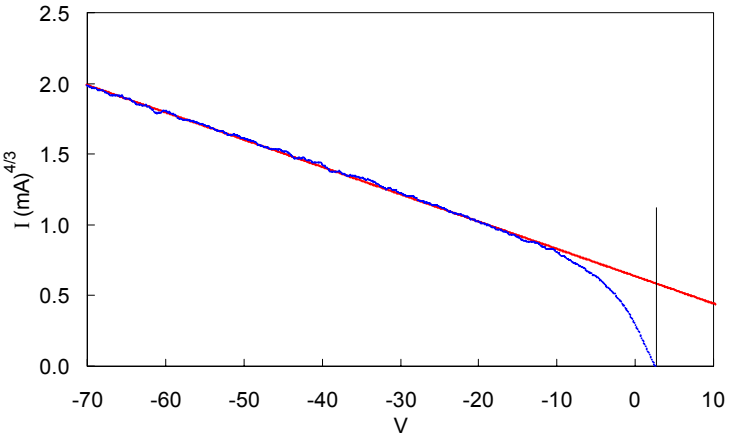

Fig. 36. Extrapolation of an $I^{4/3}$-V curve to the floating potential.

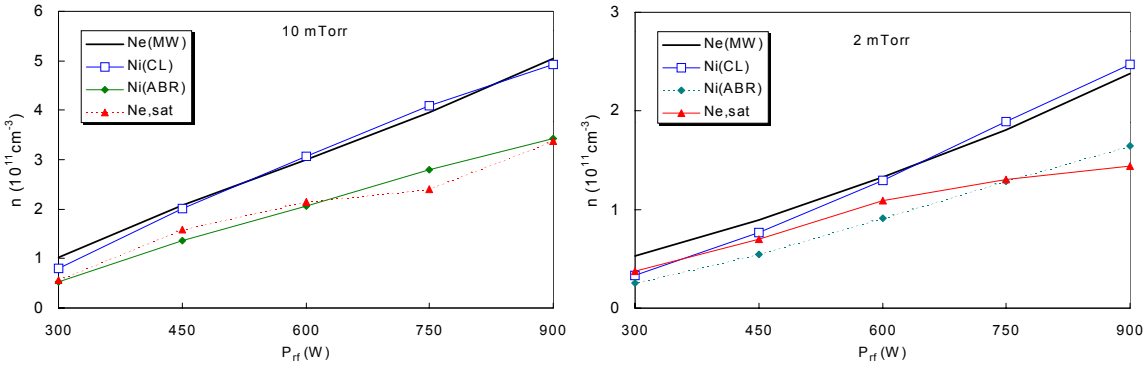

Fig. 37. Comparison of the accuracy of the floating potential, ABR, and *E*sat methods.

probes. When the FP method is formulated to include cylindrical effects, it is essentially the same as the ABR theory. The neglected effects are 1) orbiting of ions around the probe, 2) the density of electrons in the sheath, and 3) escape of ions along the probe axis. This last effect is illustrated in Fig. 38. It is almost always overlooked but fortunately is often small.

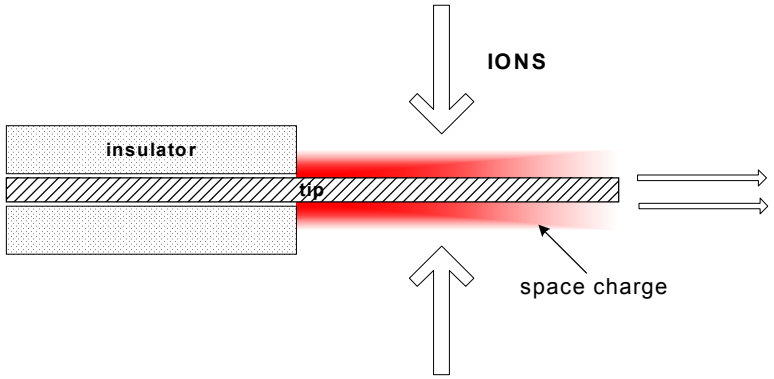

Fig. 38. Ions converging to a cylinder create a large positive space charge. For a finite-length probe, this space charge creates an electric field along the axis which can remove ions before they are collected.

An Excel program for analyzing an $I - V$ curve using the FP method is available on the author's website[15] under Presentations. Since only straight-line fits are needed, this program is very fast and can analyze a 1000-point $I - V$ curve in << 1 sec, provided that the curve is well behaved.

5. Low density rf plasmas

We have seen that the OML theory for cylinders predicts a parabolic $I_i - V$ curve, where I_i^p varies linearly with V_p, with $p = 2$. The ABR theory has this behavior at low ξ_p, and a flatter curve, $p > 2$, at high ξ_p. The BRL theory also predicts a more saturated curve than $p = 2$. In the previous section, we saw that in rf plasmas the ion current saturates less well, with $p \approx 3/2$. The FP method can show such a dependence, but that method has no theoretical justification. At even lower densities of $10^{7\text{-}9}$ cm^{-3}, rf plasmas show no ion saturation at all, and I_{sat} grows linearly with V_p. An example of this is shown in Fig. 39, from a 2-mTorr argon rf discharge with n in the 10^8 cm^{-3} range. This behavior could be due to charge exchange collisions, as explained in paragraph 3 above, but it is surprising that the curve is so nearly linear and that it is found at such low pressures. This regime requires more investigation.

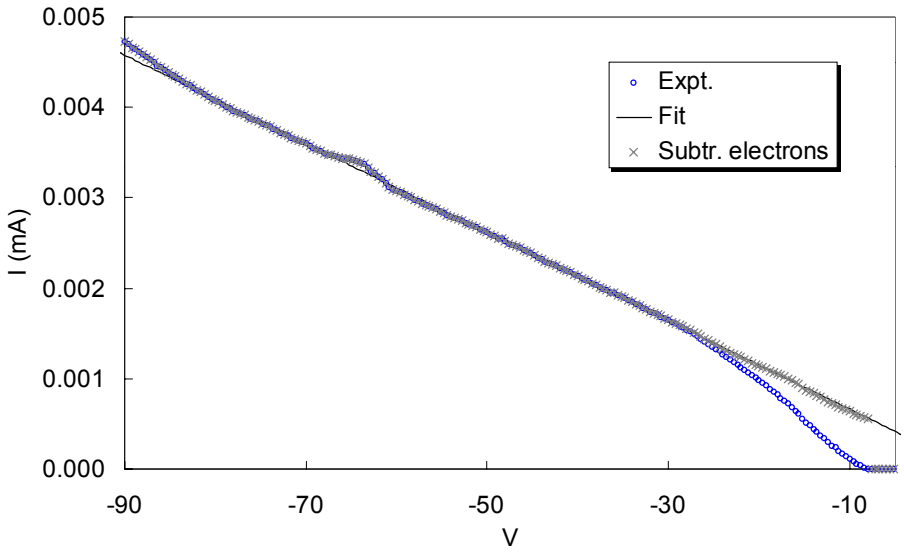

Fig. 39. Ion current vs. V_p in a very low density rf plasma. The bottom curve is the raw data. The data with the electron current removed fits a straight line.

IV. SAMPLE ANALYSES OF EXPERIMENTAL RESULTS

A. A typical RF plasma

As Fig. 40 shows, partially ionized rf plasmas typically have poor electron saturation and a very indistinct "knee" of the $I - V$ curve. In this case, however, we are fortunate that the knee at least is smooth, yielding the dI/dV curve shown in Fig. 5. Drawing a smooth line

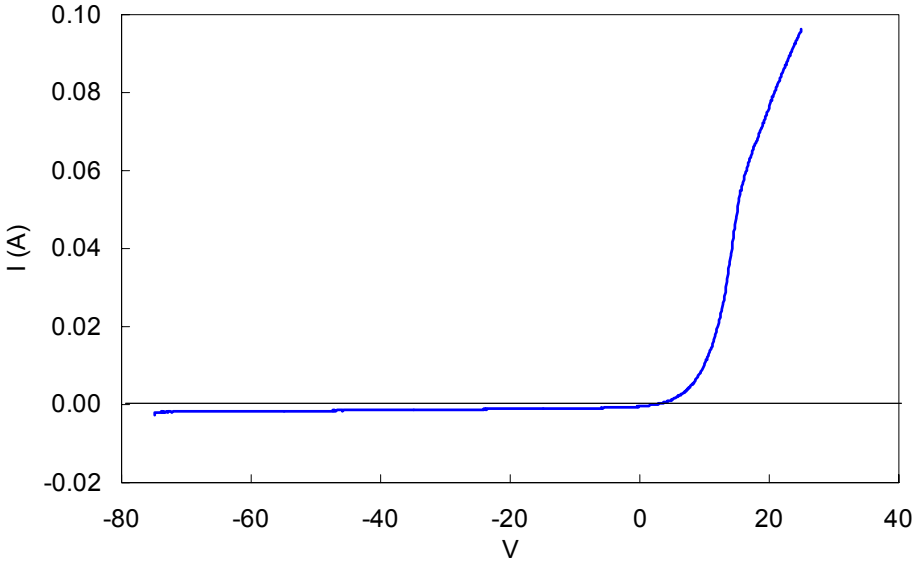

Fig. 40. A typical $I - V$ curve from an rf plasma.

through that curve yields a value for the space potential V_s, though I_e has not really saturated there. Another example of the dI/dV curve is shown in Fig. 41. Here the function I/(dI/dV) is also plotted. As seen from Eq. (1), this function is simply T_{eV}, plotted on the right scale in Fig. 41. For a Maxwellian distribution, this curve should be flat in the exponential region of

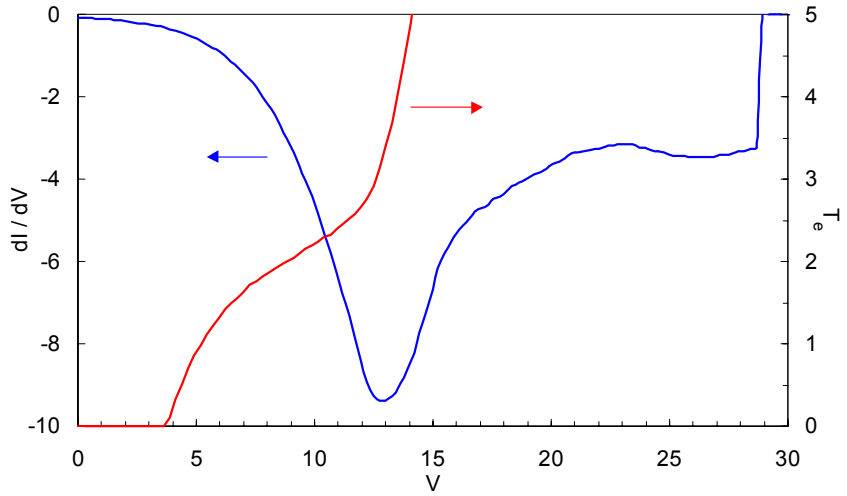

Fig. 41. Plots of dI/dV and I/(dI/dV).

the $I - V$ curve, just to the left of V_s. Fig. 41 shows only a slight flattening of the T_{eV} curve there, at a T_{eV} value of about 2 eV. The next step is to plot I_i in such a way that it can be extrapolated. This is shown in Figs. 35 and 36. The exponent p in the I^p–V curve is chosen to be 2, 4/3, 1, or whatever value fits best. The BRL or ABR curves will not fit a simple power law; an example is shown in Fig. 42. In such a case, the theoretical curve is adjusted by varying n for values of V_s and T_{eV} found from other parts of the $I - V$ curve.

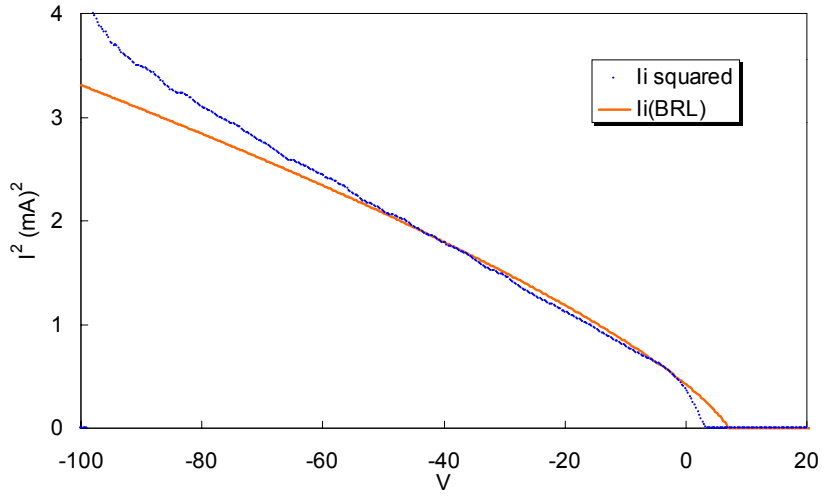

Fig. 42. Fit of ion data to a BRL curve.

Next, the extrapolated ion fit is subtracted from the electron current to give better data for the semilog electron curve, Fig. 1. If the I_i fit is good and the extrapolation is valid, the transition region should be linear over a much wider range of V_p, as seen in Fig. 1. This yields a good value of KT_e. Knowing V_s and KT_e, one can compute η [Eq. (24)] for use in calculating the jparametrized I_{sat} curves. This process can be iterated, with the ion fit affecting the electron data, and the T_{eV} value from I_e affecting the computed ion curves. The mechanism for this iteration can be set up on computer programs[15], but in most cases the fitting has to be tended manually using experienced judgment. Only the floating potential method works well automatically.

B. Example of a problematic probe curve

A very low densities $I - V$ curves that do not have the classical shape can be found. An example is shown in Fig. 43, which seems to have no exponential region and no electron saturation. The ion characteristic was shown in Fig. 39, where it is seen that I_{sat} grows linearly with bias voltage. When shown on an amplified scale (Fig. 44), it is apparent that the ion current is affected by collection of a fast electron population. To characterize these fast

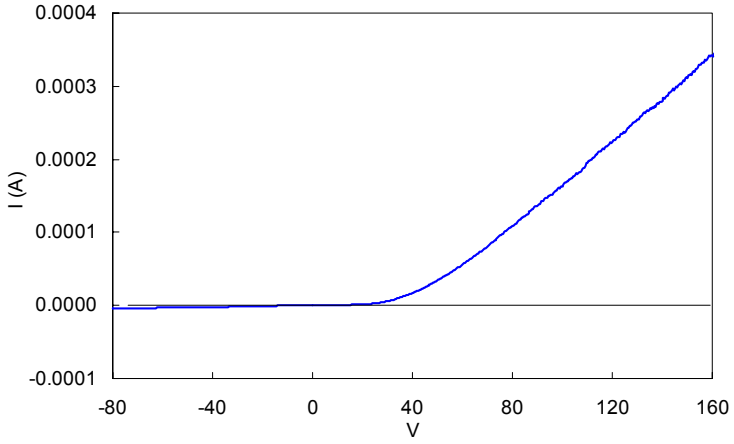

Fig. 43. An non-standard $I - V$ curve seen at low density.

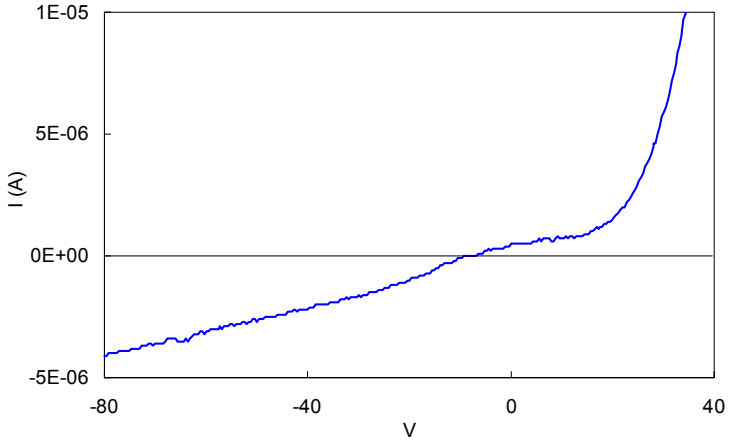

Fig. 44. $I - V$ curve near V_f, showing presence of fast electrons.

electrons, we first fit a line to I_{sat} on Fig. 39 between –90 and –30 V to remove the ions from I_e. The relevant portion of the corrected I_e curve is shown in Fg. 45. We can try to fit it with

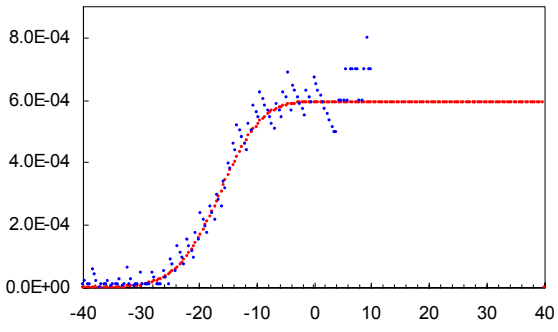

Fig. 45. The bump in the electron distribution.

a drifted Maxwellian of the form

$$f(v) = \left(\frac{m}{2\pi KT_b}\right)^{1/2} \exp\left[-m(v-v_b)^2/2KT_b\right], \tag{31}$$

where the subscript *b* refers to the "beam". To reach the probe biased at V_p, an electron must have a velocity exceeding a critical velocity v_c given by

$$\tfrac{1}{2}mv_c^2 = -e(V_p - V_s), \quad v_c = [-2e(V_p - V_s)/m]^{1/2}. \tag{32}$$

For simplicity we can set $V_s = 0$ here and shift the axis back later. We now define

$$v_{thb} \equiv (2KT_b/m)^{1/2}, \qquad u \equiv v/v_{thb}. \tag{33}$$

For a probe of area *S* and a beam density of n_e, the beam current to a probe at V_p is then

$$\begin{aligned} I_b &= en_bS\int_{v_c}^{\infty} f(v)v\,dv \\ &= en_bS\left(\frac{m}{2\pi KT_b}\right)^{1/2}\int_{u_c}^{\infty} e^{-(u-u_b)^2} v_{thb}^2 u\,du \\ &= en_bS\left(\frac{2KT_b}{\pi m}\right)^{1/2}\int_{u_c}^{\infty} e^{-(u-u_b)^2} u\,du \equiv I_0\int_{u_c}^{\infty} e^{-(u-u_b)^2} u\,du \end{aligned} \tag{34}$$

where I_0 is the dimensional constant before the integral. The integral can be evaluated numerically, or it can be expressed in terms of an error function:

$$I_b = \frac{I_0}{2}\left\{e^{-x_c^2} + u_b\sqrt{\pi}\left[1 \mp \mathrm{erf}(|x_c|)\right]\right\}, \quad \begin{matrix} x_c > 0 \\ x_c < 0 \end{matrix}. \tag{35}$$

The solid curve in Fig. 45 shows a fit of this function to the data, requiring a beam of energy 56 eV and temperature 0.3 eV — a rather narrow fast electron population.

A semilog plot of the electron characteristic is shown in Fig. 46. The beam is much more apparent when the extrapolated ion current is removed. However, a line through the exponential part of the curve yields an unreasonably high value of $KT_e = 7.6$ eV. To get the correct T_e, we must subtract the beam current, given by Eq. (35), The result is shown in Fig. 47. The Maxwellian portion now corresponds to $KT_e = 4.8$ eV, which could be true at these low densities. The beam and thermal fits were then further tweaked so that the curve of their sum (the faint, broad curve) fit the data at the junction point. Conclusion: a false value of KT_e can result from simply drawing a straight line through the curve of Fig. 46.

At high positive V_p, it would appear from Fig. 46 that I_e reaches saturation, but clearly the onset is far below V_s, since the transition region is so short. When I_e is plotted on a linear scale (Fig. 48) it is clear that I_e does not saturate at all: it increases linearly with V_p. Since the density is low and the sheath thick, orbital theory should obtain here. According to the

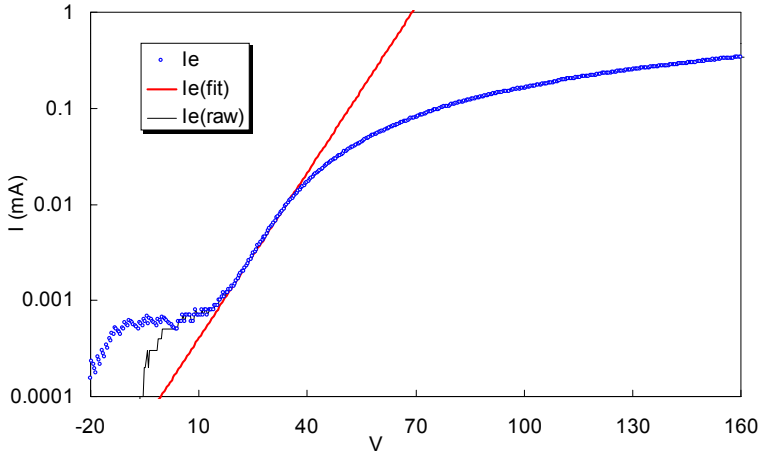

Fig. 46. The electron current on a semilog plot. The thin solid curve is the raw data including the ions. The straight line is a fit to the exponential part.

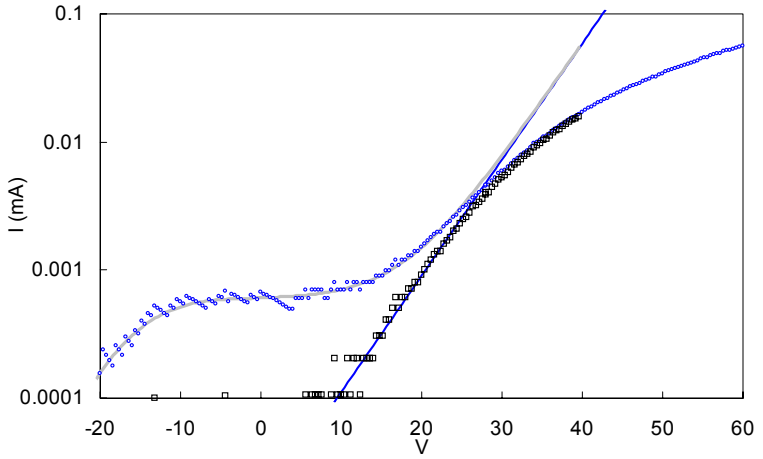

Fig. 47. The electron current with ions subtracted (○) and with the beam also subtracted (□). The straight line is a fit to the short exponential section. The faint curve is the sum of this fit and the fit to the fast electron component.

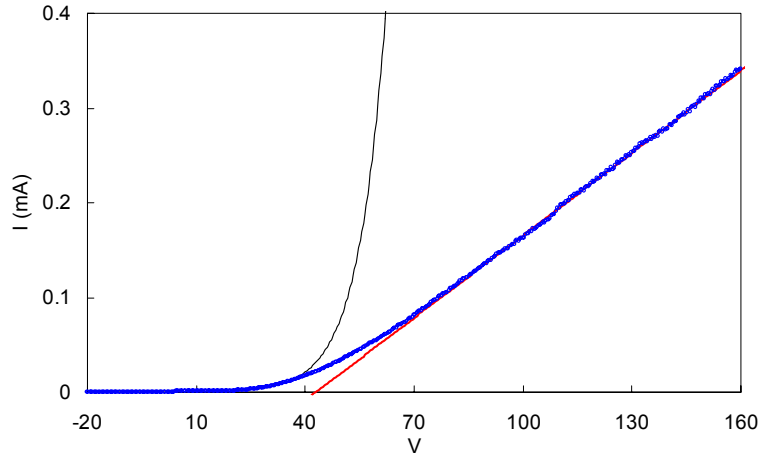

Fig. 48. Electron characteristic on a linear scale. The data in the saturation region fit a straight line closely. The curve is an exponential fit to the Maxwellian region.

electron counterpart to Eq. (22), E_{sat} should be proportional to $V^{1/2}$. A linear increase is more characteristic of a spherical probe. In this case, the probe is very long and thin, so that even if the sheath becomes as large as the probe length, I_e should have a portion $\propto V^{1/2}$ when $R_p < d < L$. Another unlikely reason is that the probe is drawing more electron current than the total ion current to the chamber walls. In that case, the plasma cannot remain quasineutral unless V_s rises to drive more ions into the wall. Linear E_{sat} is then a reflection of the linearity of the I_{sat} curve (which is not understood). This problem of wall sheath impedance has been discussed by Godyak et al.[26,27] A dirty probe with a coating on the surface could also give spurious $I - V$ curves. Conclusion: there are Langmuir probe curves which do not have the classical shape and require extraordinary treatment.

V. SPECIAL TECHNIQUES

A. Distribution functions

Since the ion current is not sensitive to T_i, Langmuir probes cannot measure ion temperature, and certainly not the ion velocity distribution. However, careful measurement of the transition region of the $I - V$ characteristic can reveal the electron distribution if it is isotropic. If the probe surface is a plane perpendicular to x, the electron flux entering the sheath depends only on the x component of velocity, v_x. For instance, the Maxwell distribution for v_x is

$$f_M(v_x) = \left(\frac{1}{v_{th}\sqrt{\pi}}\right)\exp(-v_x^2/v_{th}^2), \qquad v_{th}^2 \equiv 2KT_e/m. \tag{36}$$

The coefficient normalizes $f(v)$ so that its integral over all v_x's is unity. If $f(v)$ is not Maxwellian, it will have another form and another coefficient in front. The electron current that can get over the Coulomb barrier and be collected by the probe will therefore be

$$I_e = eAn\int_{v_{min}}^{\infty} v_x f(v_x)dv_x\ , \quad \tfrac{1}{2}mv_{min}^2 = e(V_s - V_p) = -eV_p\,, \tag{37}$$

where v_{min} is the minimum energy of an electron that can reach the probe, and $V_s = 0$ by definition. Taking the derivative and simplifying, we find

$$\frac{dI_e}{dV_p} = eAn\frac{d}{dV_p}\int_{v_{min}}^{\infty} v_x f(v_x)\frac{dv_x}{dV_p}dV_p = -eAn\,v_x f(v_x)\frac{dv_x}{dV_p}\bigg|_{v_x=v_{min}}$$

$$= -eAn\,v_x f(v_x)\frac{-e}{mv_x}\bigg|_{v_x=v_{min}} = A\frac{ne^2}{m}f(v_{min})\,, \tag{30}$$

so that $f(v_x)$ can be found from the first derivative of the $I - V$ curve. If the probe is not flat, however, one has to take the three-dimensional distribution $g(v) = 4\pi v^2 f(v)$, where v is the absolute value $|v|$ of the velocity, and take into account the various angles if incidence. Without going into the details, we then find, surprisingly, that $f(v)$ is proportional to the *second* derivative of the $I - V$ curve:

$$\frac{d^2 I_e}{dV_p^2} \propto f(\mathrm{v}) \tag{31}$$

This result is valid for any convex probe shape as long as the distribution is isotropic, and for any anisotropic distribution if the probe is spherical. To differentiate $I - V$ data twice will yield noisy results unless a good deal of smoothing is employed. Alternatively, one can *dither* the probe voltage by modulating it at a low frequency, and the signal at the dither frequency will be proportional to the first derivative. In that case, only one further derivative has to be taken to get $f(\mathrm{v})$. Figure 49 is an example of non-Maxwellian $f(\mathrm{v})$'s obtained by double differentiation with digital filtering.

In special cases where the EEDF consists of two Maxwellians with well separated temperatures, the two KT_e's can be obtained by straight-line fits on the semilog $I - V$ curve without complicated analysis. An example of this is shown in Fig. 50.

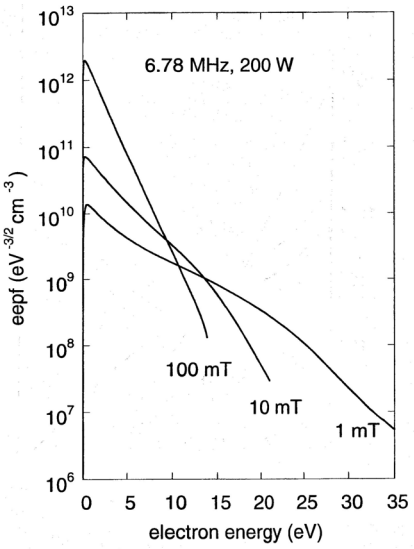

Fig. 49. EEDF curves obtained with a Langmuir probe in a TCP discharge (Ref. 27).

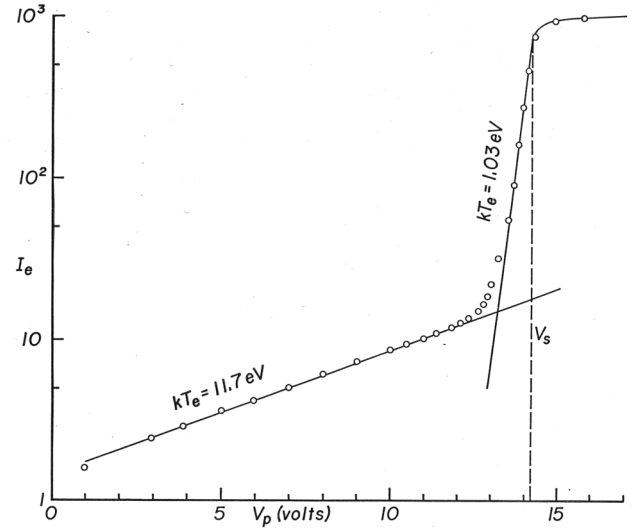

Fig. 50. An $I - V$ curve of a bi-Maxwellian EEDF.

B. Double probes and hot probes

When V_s fluctuates slowly, one can use the method of double probes, in which two identical probes are inserted into the plasma in close proximity, and the current from one to the other is measured as a function of the voltage difference between them (*c.f.* Chen, *loc. cit.*). The $I - V$ characteristic is then symmetrical and limited to the region between the I_{sat}'s on each probe. If the probe array floats up and down with the rf oscillations, the $I - V$ curve should not be distorted. However, it is almost impossible to make the whole two-probe system float at rf frequencies because of the large stray capacitance to ground. Even if both tips are rd compensated, the rf impedances must be identical. Nonetheless, many industrial plasmas have no contact with a grounded electrode, and a double probe has to be used, sometimes successfully.

Hot probes are small filaments that can be heated to emit electrons. These electrons, which have very low energies corresponding to the KT of the filament, cannot leave the probe as long as V_p - V_s is positive. As soon as V_p - V_s goes negative, however, the thermionic current leaves the probe, and the probe current is dominated by this rather than by the

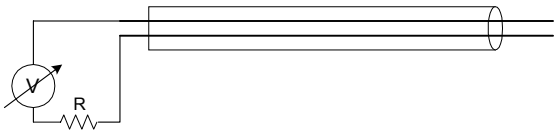

Fig. 51. A double probe.

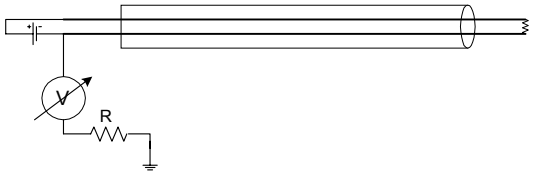

Fig. 52. A hot probe.

ion current. Where the $I - V$ curve crosses the x axis, therefore, is a good measure of V_s. The voltage applied to the filament to heat it can be eliminated by turning it off and taking the probe data before the filament cools. One can also heat the probe by bombarding it with ions at a very large negative V_p, and then switching this voltage off before the measurement. In general it is tricky to make hot probes small enough. For further information on these techniques, the reader is referred to the chapter by Hershkowitz (*loc. cit.*).

C. Capacitively coupled probes

Though most laboratory experiments are done in an inert gas like argon or helium, rf plasmas used in industry have reactive gases, which can wreak havoc on a Langmuir probe. A common problem is that the probe surface becomes coated with an insulating layer. Booth et al[28]. have devised a transient probe to circumvent this problem. The circuit is shown in Fig. 53a. A large rf pulse is applied through the back-to-back diodes and external capacitor C_x to a coated flat probe. The equivalent circuit is shown in Fig. 53b, where Z_{sh} is the sheath impedance, C_f is the capacitance of the film across which the potential drops from V_{surf} to V_c, and the C_p's are stray capacitances. The rf pulse applies a negative dc voltage to the film surface by the sheath rectification effect. After the rf is turned off, this voltage decays through C_f and C_x, providing a probe bias sweep. The instantaneous V_p is measured at C with a high-impedance probe. The current is measured with the resistor R.

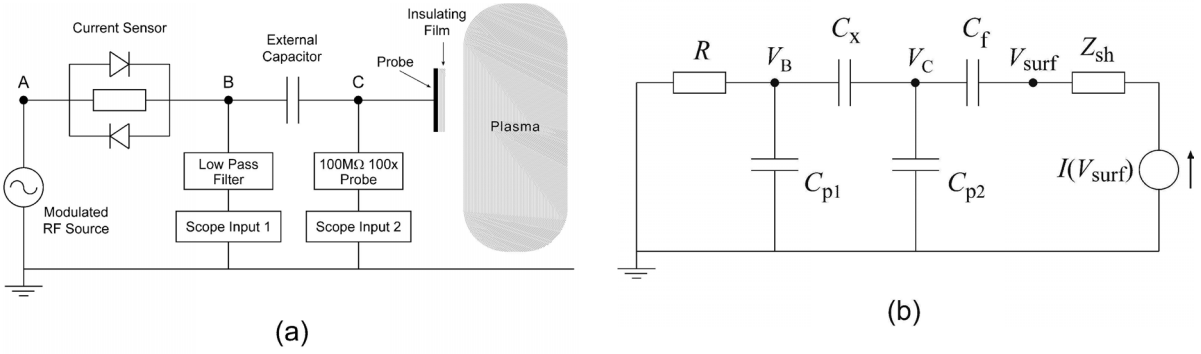

Fig. 53. Circuit for transient flat probe (Ref. 28).

With the proper value of C_x, an entire $I - V$ curve can be swept out in a few milliseconds. As the film grows in thickness, C_f decreases, and the probe $I - V$ will decay at a faster rate, as shown in Fig. 54. C_x must be adjusted accordingly. When the film becomes too thick, the sweep will be too fast for the sheath to come to equilibrium. Figure 5 shows a normal ion characteristic obtained with this technique. However, a guard ring (Fig. 11) must be used and adjusted properly. Figure 56a shows the effect of the guard ring, and Fig. 56b shows that the $I - V$ curve behaves properly with pressure.

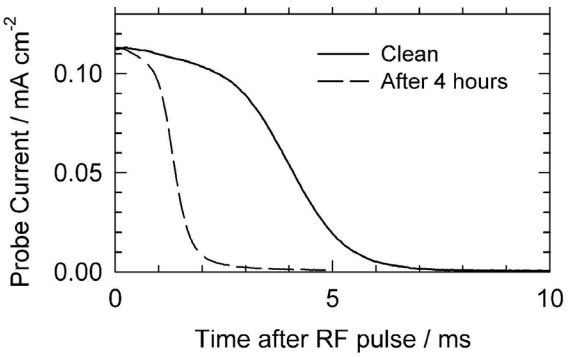

Fig. 54. Change of decay rate with C_f.

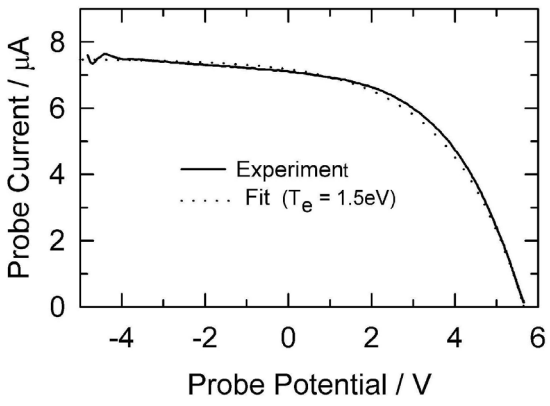

Fig. 55. *I – V* curve with transient probe.

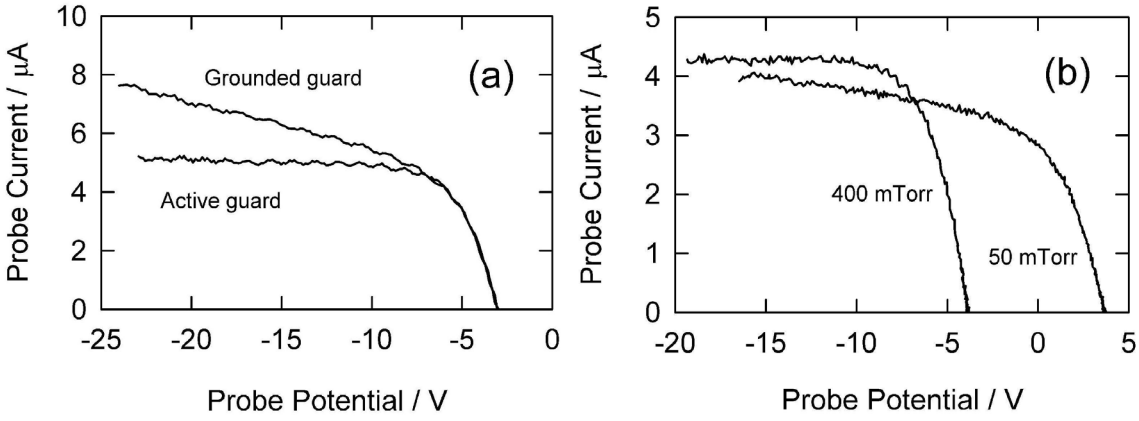

Fig. 56. *I – V* curves vs. (a) guard ring voltage and (b) pressure.

REFERENCES

[1] F.F. Chen and J.D. Evans, unpublished data.

[2] I.D. Sudit and R.C. Woods, Rev. Sci. Instrum. **64**, 2440 (1993).

[3] F.F. Chen, *Introduction to Plasma Physics and Controlled Fusion*, 2nd ed., Vol. 1:, p. 292 (Plenum Press, New York, 1984).

[4] F.F. Chen, J.D. Evans, and D. Arnush, Phys. Plasmas **9**, 1449 (2002).

[5] N. Hershkowitz, *loc. cit*., p. 146.

[6] S.V. Ratynskaia, V.I. Demidov, and K. Rypdal, Rev. Sci. Instrum. **71**, 1367 (2000).

[7] I.D. Sudit and F.F. Chen, Plasma Sources Sci. Technol. **3**, 162 (1994).

[8] F.A. Haas, A. Goodyear, and N. St..J. Braithwaite, Plasma Sources Sci. Technol. **11**, 544 (2002).

[9] F.F. Chen,, Phys. Plasmas **8**, 3029 (2001).

[10] R.N. Franklin, IEEE Trans. Plasma Sci. **30**, 352 (2002).

[11] V. Godyak and N. Sternberg, IEEE Trans. Plasma Sci. **31**, 303.

[12] I.D. Kaganovitch, Phys. Plasmas **9**, 4788 (2002).

[13] J.E. Allen, Phys. Plasmas **10**, 1528 (2003).

[14] H. Mott-Smith and I. Langmuir, Phys. Rev. **28**, 27 (1926).

[15] www.ee.ucla.edu/~ltptl

[16] J.E. Allen, R.L.F. Boyd, and P. Reynolds, Proc. Phys. Soc. (London) **B70**, 297 (1957).

[17] F.F. Chen, J. Nucl. Energy, Pt. C **7**, 47 (1965).

[18] F.F. Chen, J.Appl. Phys. **36**, 675 (1965).

[19] I.B. Bernstein, and I.N. Rabinowitz, Phys. Fluids **2**, 112 (1959).

[20] Laframboise, J.G. 1966 Univ. Toronto Inst. Aerospace Studies Rept. 100 (June, 1966).

[21] F.F. Chen, C. Etievant, and D. Mosher, Phys. Fluids **11**, 811 (1968).

[22] Z. Sternovsky, S. Robertson, and M. Lampe, Phys. Plasmas **10**, 300 (2003).

[23] Z. Sternovsky, S. Robertson, and M. Lampe, *Ion collection by cylindrical probes in weakly collisional plasmas: theory and experiment*, J. Appl. Phys. (to be published).

[24] M.A. Lieberman and A.J. Lichtenberg, *Principles of Plasma Discharges and Materials Processing* (Wiley, New York, 1994), p. 165 or F.F. Chen, *Introduction to Plasma Physics and Controlled Fusion*, 2nd ed., Vol. 1 (Plenum Press, New York, 1984), p 294.

[25] F.F. Chen, J.D. Evans, and D. Arnush, Phys. Plasmas **9**, 1449 (2002).

[26] V.A. Godyak, R.B. Piejak, and B.M. Alexandrovich, J. Appl. Phys. **69**, 3455 (1991).

[27] V.A. Godyak, R.B. Piejak, and B.M. Alexandrovich, Plasma Sources Sci. Technol. **11**, 525 (2002).

[28] J.P. Booth, N. St. J. Braithwaite, A. Goodyear, and P. Barroy, Rev. Sci. Instrum. **71**, 2722 (2000).